



**HAL**  
open science

## Use of the sent specimen in pipeline design

Clement Soret, Yazid Madi, Jacques Besson, Vincent Gaffard

► **To cite this version:**

Clement Soret, Yazid Madi, Jacques Besson, Vincent Gaffard. Use of the sent specimen in pipeline design. 20th JTM - EPRG European pipeline research group, May 2015, Paris, France. 34 p. hal-01183303

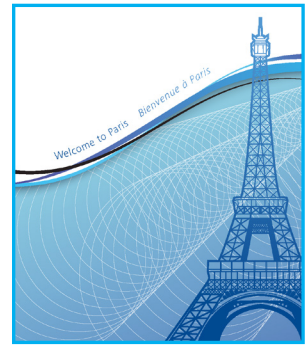
**HAL Id: hal-01183303**

**<https://minesparis-psl.hal.science/hal-01183303>**

Submitted on 7 Aug 2015

**HAL** is a multi-disciplinary open access archive for the deposit and dissemination of scientific research documents, whether they are published or not. The documents may come from teaching and research institutions in France or abroad, or from public or private research centers.

L'archive ouverte pluridisciplinaire **HAL**, est destinée au dépôt et à la diffusion de documents scientifiques de niveau recherche, publiés ou non, émanant des établissements d'enseignement et de recherche français ou étrangers, des laboratoires publics ou privés.



## Paper 29

### USE OF THE SENT SPECIMEN IN PIPELINE DESIGN

**Clement Soret\*, Yazid Madi and Jacques Besson**  
Centre des Materiaux P.-M. Fourt, Mines Paristech, Paris, France.

**Vincent Gaffard**  
TOTAL Exploration & Production, Paris La Defense, France.

\* Presenting author

#### ABSTRACT

Engineering critical assessments have been developed based on fracture mechanics principles to determine whether or not a given flaw is safe from failure under specified loading conditions. Several parameters are required as inputs, such as the geometry of the flaw, the stress acting at the vicinity of the flaw and the material properties (toughness, tensile properties). To do so, advanced fracture-mechanics testing (critical  $K$ , CTOD or  $J$ ) are usually required to guarantee an accurate measurement of the material toughness.

It is accepted that the Compact Tension (CT) and the Single-Edge Notched Bending (SENB) may lead to unnecessary conservatism in safety assessments. The Single-Edge Notched Tensile (SENT) specimen could be the most acceptable substitute since it is shown to lead to less conservatism.

This paper consists of three parts. First, the transferability between laboratory specimens and a pipe is studied in terms of  $J$ - $Q$  approach. It is shown that the CT and SENB specimens, which are both loaded in bending, do not well represent the constraint at the vicinity of the crack tip in a pipe and are over-conservative. However, the SENT specimen presents a very good transferability with regards to the pipe.

In a second part, results of the SENT tests are presented and a comparison between existing tests protocols is proposed. More specifically, the specimen pre-cracking procedure is studied.

The third part is dedicated to engineering critical assessments based on the SENT test results using either a CTOD approach or a R-curve approach (BS-7910:2005 [1], DNV-RP-F108 [2]), tangency analysis approaches and a local approach to fracture based on the continuum mechanics of porous media (Gurson Tvergaard Needleman damage model).

## 1. INTRODUCTION

The through process of an engineering critical assessment is described in Figure 1 below.

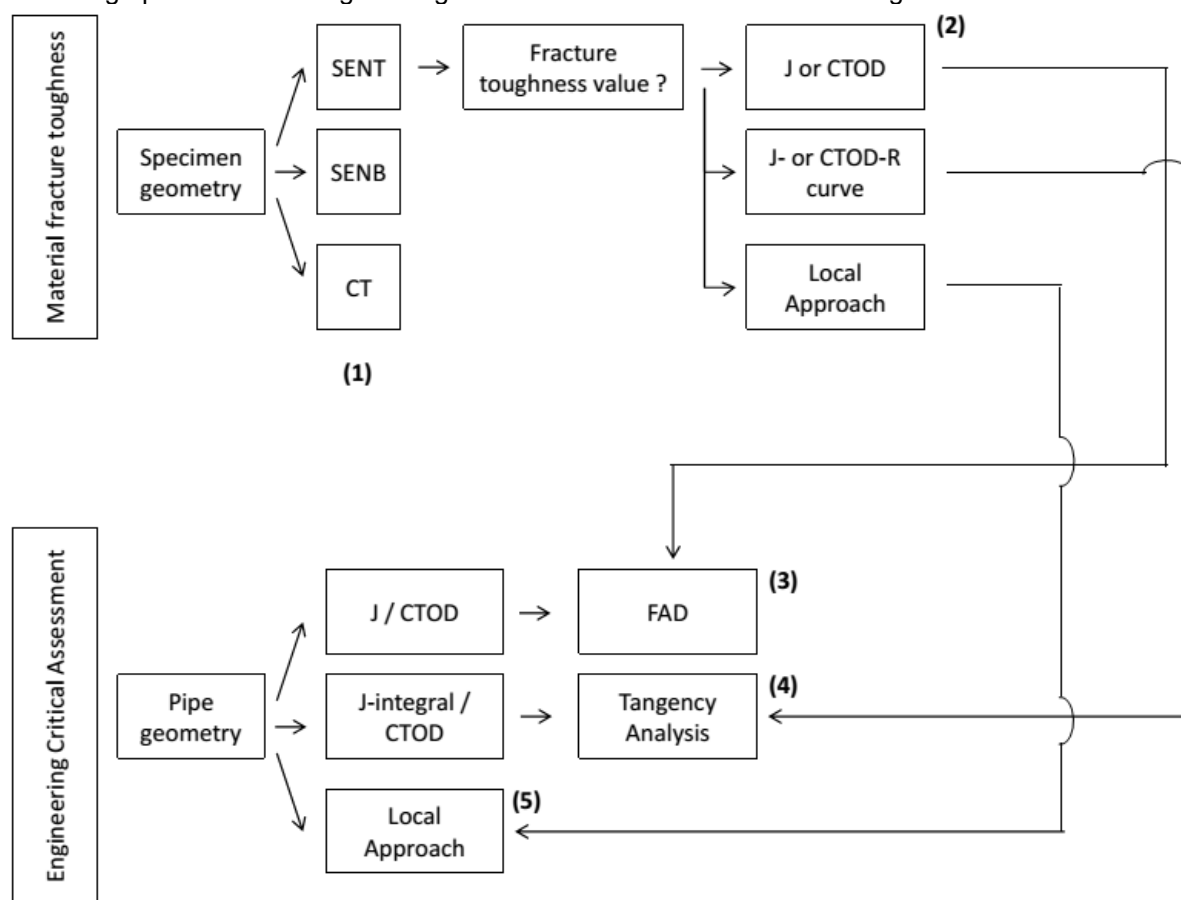


Figure 1 - Flow chart describing the engineering critical assessment through process

The objective of this paper is to highlight and discuss within this overall process some critical points.

(1) with reference to Figure 1.

The material properties are compulsory inputs for the assessment of flaws in pipelines. The classical mechanical values (such as the Young's modulus  $E$ , the Poisson's ratio  $\nu$ , the yield stress  $\sigma_Y$ , the ultimate strength  $\sigma_{UTS}$ , and others) are determined through standardized tensile tests, as described in ASTM A370 [3] and DNV-OS-F101 [4]. However, the determination of the material toughness requires more engineering judgment. Indeed, all the engineering critical assessment stem up on the assumption that the transferability of the fracture mechanics parameters ( $K$ ,  $J$ ,  $CTOD$ ) exists between a pipeline tube and the laboratory specimen used for the tests. Also, it is important to chose with discernment the best specimen geometry.

The most common specimens for toughness tests are the Cracked Tensile (CT) specimens and the Single-Edge Notched Bending (SENB) specimens, and their use is described in international standards, namely the ASTM E1820 [5] and the BS-7448 [6]. These specimens are both deep cracked ( $a_0/W \approx 0.5-0.7$ ) and subjected to a bending load. It results in a high crack-tip constraint condition, unrepresentative of a surface crack in a pipe.

As a remedy, the Single-Edged Notched Tensile (SENT) specimen was introduced. Subjected to a tensile load, this specimen presents a low crack tip constraint condition, as shown by previous numerical studies.

In this paper, the transferability of the CT, SENB and SENT specimens to the pipe is studied on the basis of the  $J$ - $Q$  approach. Results are discussed in **section 2**, and confirm the ability of the SENT

specimen to be representative of the pipe for low and high  $D/t$  ratios and for both uniaxial and biaxial loading conditions.

Since no standard normalizes the use of the SENT specimen, the test procedure is also not straightforward. In **section 3**, an overview of the existing recommended practices (DNV, CanMet, ExxonMobil) is proposed. In particular, it is shown that the non-uniqueness of the specimen geometry, the testing conditions and others requirements result in a test that may lead to unnecessary under- or over-conservative fracture toughness values and  $J$ - or CTOD-R curves.

(2) with reference to Figure 1.

The definition of the fracture mechanics tests conditions and the analysis of the test results raise some questions:

- the impact of the  $a/W$  ratio on the test results (CTOD/ $J$  value and CTOD/ $J$ -R curve)
- the question of the relevant parameter to be considered:  $J$  or CTOD and the transferability from  $J$  to CTOD and vice-versa
- the question of the selection of the experimental method for CTOD determination: double clip or optical measurement by use of Digital Image Correlation (DIC).
- the relevant method for the  $J$ -R curve determination. In particular the use of multiple vs. one test specimen testing.

(3) with reference to Figure 1.

The Failure Assessment Diagram (FAD) approach is standardized in BS 7910 and API 579. The approach has been extended to strain based design applications in DNV OS F101 and DNV RP F108.

The main steps of the methodology are reminded in section 4 where issues related to the FAD for high  $L_r$  values are also discussed.

(4) with reference to Figure 1.

Tangency analysis is based on the experimental determination of the R-curve on one side ( $J$  or CTOD R-curve) and finite element calculations of the crack driving force on the other side.

The calculation of the crack driving force raises questions regarding:

- the 3D determination of the  $J$ -integral in the elastic plastic domain. Some checks performed with Abaqus show that FE codes may fail in the determination of the  $J$ -integral. Where CTOD is used (as proposed by ExxonMobil) transferability from SENT specimen to the pipe and method for CTOD determination in Finite Element calculations shall be carefully addressed.
- the impact of neglecting the accumulated plastic strain at the crack tip for the determination of the crack driving force.

(5) with reference to Figure 1.

Local approach to fracture allows predicting pipe material and welds behaviour with reducing significantly the questions of transferability between the lab specimens and the structure. However, it requires performing tests on various specimen geometries to account for the effects of stress triaxiality ratio on damage and fracture behaviour. In particular, notched tensile specimens (which are not standardised tests today) are required.

In section 7.3, the tests which need to be performed are described. The model identification procedure is detailed. Then the model is validated on SENT tests specimens before being used on pipes for ECA.

Finally, a review of the three described ECA approaches (FAD, Tangency analysis and local approach) based on the SENT specimen is addressed in the sections 7.5 to 7.8.

## 2. TRANSFERABILITY OF THE SENT SPECIMENS TO THE PIPE

### 2.1 J-Q approach

In Engineering Critical Assessments, a parameter of the fracture mechanics ( $J$  or  $CTOD$ ) calculated at the crack tip of a structure is compared to a critical value ( $J_{IC}$  or  $CTOD_C$ ) chosen as a criterion. These critical values are not only material dependent, but also depend on the specimen geometry used for their measurement. In particular, a high crack-tip constraint specimen (SENB or CT) will result on a low R-curve, whereas a low crack-tip constraint specimen (shallow SENT) will result on a higher R-curve. (see Figure 2). This qualitative ranking of the specimens shows that the SENT is particularly adapted in the case where a cracked pipe is assessed. In the following sub-section, results of a quantitative FEA based numerical analysis in terms of  $J$ - $Q$  approach are presented.

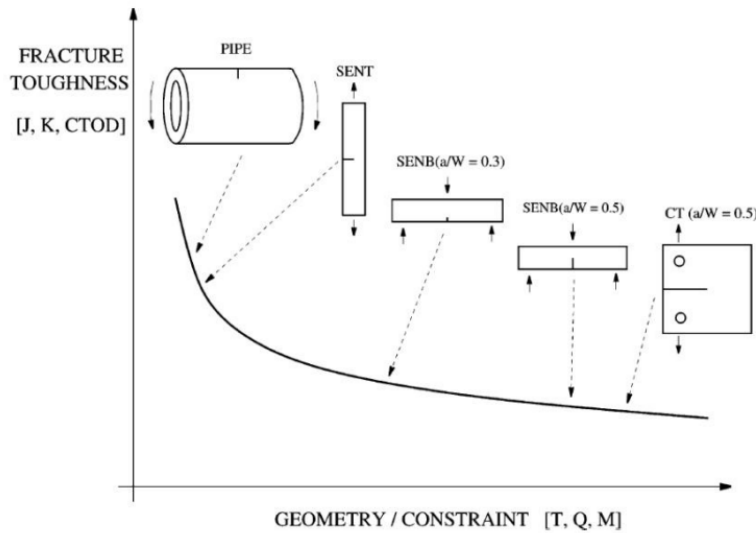


Figure 2 - Rankings of the classical fracture mechanics specimens on the  $J$ - $Q$  curve. [7]

### 2.2 J-Q approach theory

In the case of a power-law hardening material with plasticity, Hutchinson [8], Rice and Rosengren [9] showed that the stress field at the crack tip, called HRR field, writes:

$$\sigma_{ij} = \sigma_0 \left[ \frac{J}{\alpha \sigma_0 \epsilon_0 I_n r} \right]^{\frac{1}{n+1}} \bar{\sigma}_{ij}(\theta, n) \quad (1)$$

Sharma *et al.* [10] added a second order term to Eqn 1. It writes:

$$\frac{\sigma_{ij}}{\sigma_0} = \left[ \frac{J}{\alpha \sigma_0 \epsilon_0 I_n r} \right]^{\frac{1}{n+1}} \bar{\sigma}_{ij}(\theta, n) + Q \left( \frac{r \sigma_0}{J} \right)^q \bar{\sigma}_{ij}(\theta, n) \quad (2)$$

where the  $Q$  term represents the constraint effect. O'Dowd *et al.* [11] showed that Eqn 2 can be simplified in:

$$\sigma_{ij} = \left( \sigma_{ij}(r, \theta) \right)_{\text{HRR}} + Q \sigma_0 \delta_{ij} \quad (3)$$

where  $\delta_{ij}$  is the Kronecker delta. In order to respect HRR field requirements,  $Q$  values shall be calculated at a minimum distance of  $r_0 = 2J/\sigma_0$  from the crack tip, which corresponds to a distance of about four CTODs, using the equation:

$$Q = \frac{\sigma_{\theta\theta}^{FE} - \sigma_{ij}^{HRR}}{\sigma_0} \Big|_{\theta=0} \Big|_{r=\frac{2J}{\sigma_0}} \quad (4)$$

where  $\sigma_{\theta\theta}$  is calculated by finite elements analyses.

## 2.3 Finite Element Analysis

### 2.3.1 Material flow curve

A power law with Ramberg-Osgood formulation has been derived from an experimental stress strain curve. It writes:

$$\epsilon = \frac{\sigma}{E} + \alpha \frac{\sigma}{E} \left( \frac{\sigma}{\sigma_0} \right)^{n-1} \quad (5)$$

where  $n = 6.8027$ ,  $\alpha = 1$ ,  $\sigma_0 = 300$  MPa and  $E = 205$  GPa.

### 2.3.2 Specimens meshes

The simulations have been carried out using FEA Z-Set software. CT, SENB and SENT specimens have been meshed using 2D quadratic elements with reduced integration (c2d8r) and large deformations formulation, as shown in Figure 3 and Figure 4. The pipe with a long surface crack has been meshed with axisymmetric quadratic elements with reduced integration (cax8r) and large deformation formulation.  $D/t$  ratios equal to 15, 20 and 25 have been considered in order the geometry to be representative of both oil and gas transportation pipelines.

Since the calculation of the plastic confinement  $Q$  on cracked specimens requires a description of the stress near the crack tip as accurate as possible, a transition from the fine meshed region at the vicinity of the crack tip to the coarse meshed region away from the crack tip was achieved using a structured transitional mesh pattern.

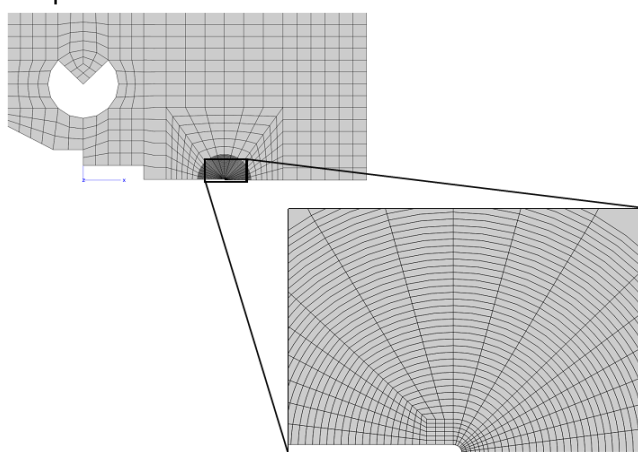


Figure 3 - 2D mesh of a CT specimen for the calculation of J-Q field. The refined mesh around the crack tip allows a accurate description of the stress field.

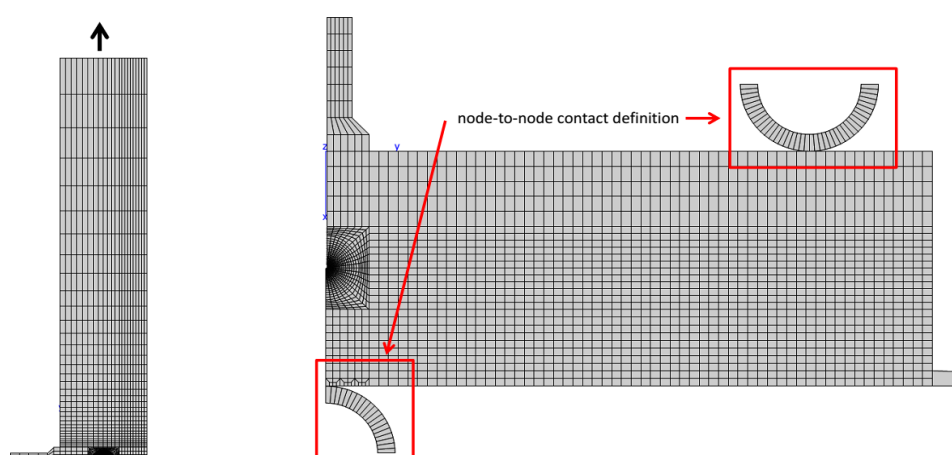


Figure 4 - 2D meshes of a SENT (left) and SENB (right) specimens for the calculation of J-Q field. The crack tips were meshed as for the CT specimen (see Figure X), and two contact areas were defined to simulate the actual loading conditions of a SENB specimen.

## 2.4 Results

Figure 5 shows the plasticity iso-value lines for the three fracture specimens for an identical load, given as a CTOD value equal to  $5 \cdot r_0$ . Here, the blue colour corresponds to areas where the cumulative plastic strain level is below 0.2%. One can clearly see that the two bended specimens (CT and SENB) show a confined plasticity with “O” shape plastic areas. In these specimens, the ligament is not fully plastic which is mainly due to the loading mode in bending. On the other hand, the pipe and SENT specimen show a generalized plasticity with a fully plastic ligament.

The different results of this numerical analysis clearly show that the SENT specimen is the best candidate for the transferability with a pipeline subjected to internal pressure and tensile, or bending. Indeed, both CT and SENB specimens present an over confined plasticity around the crack tip, which results in a lower toughness.

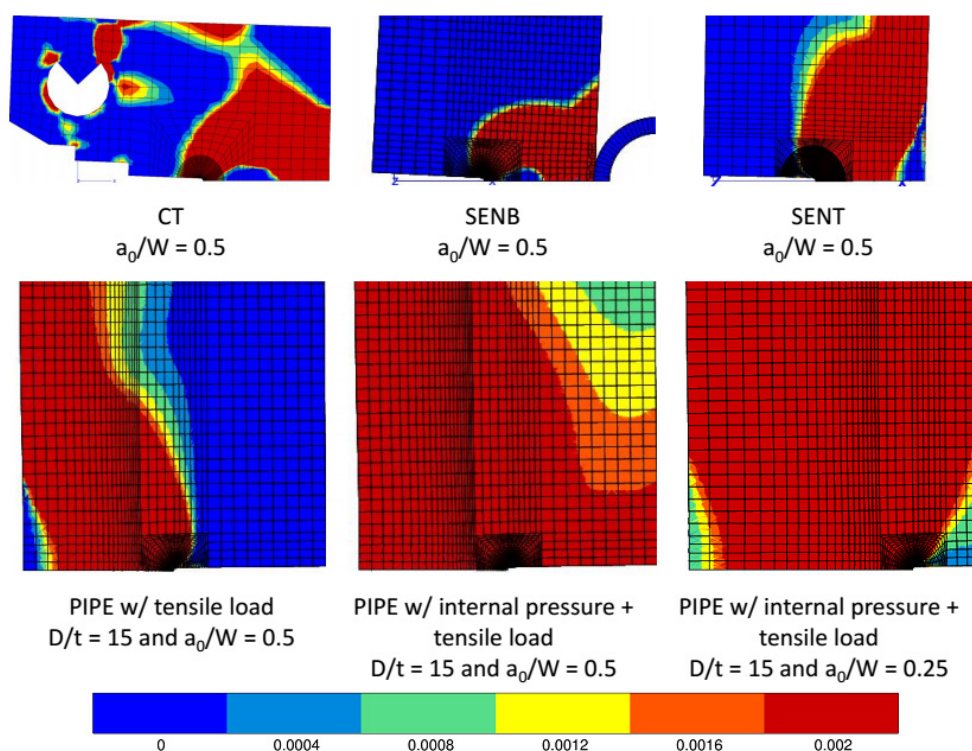


Figure 5 - Size of the cumulative plastic area calculated for the SENT, SENB and CT specimens. Comparisons are made with a pipe for an uniaxial and a biaxial load, and for  $a_0/W=0.25$  and  $a_0/W=0.5$ .

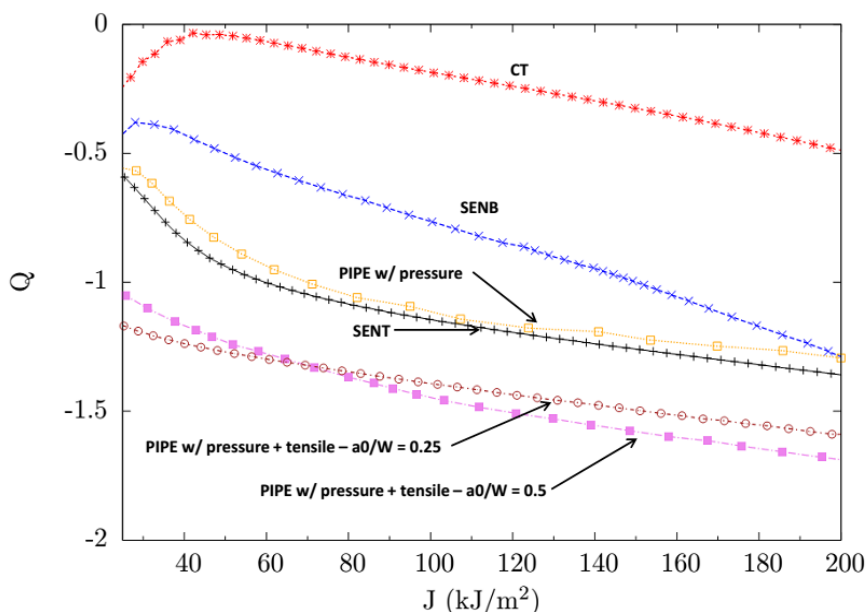


Figure 6. Evolution of the constraint  $Q$  as a function of the load expressed as  $J$ .

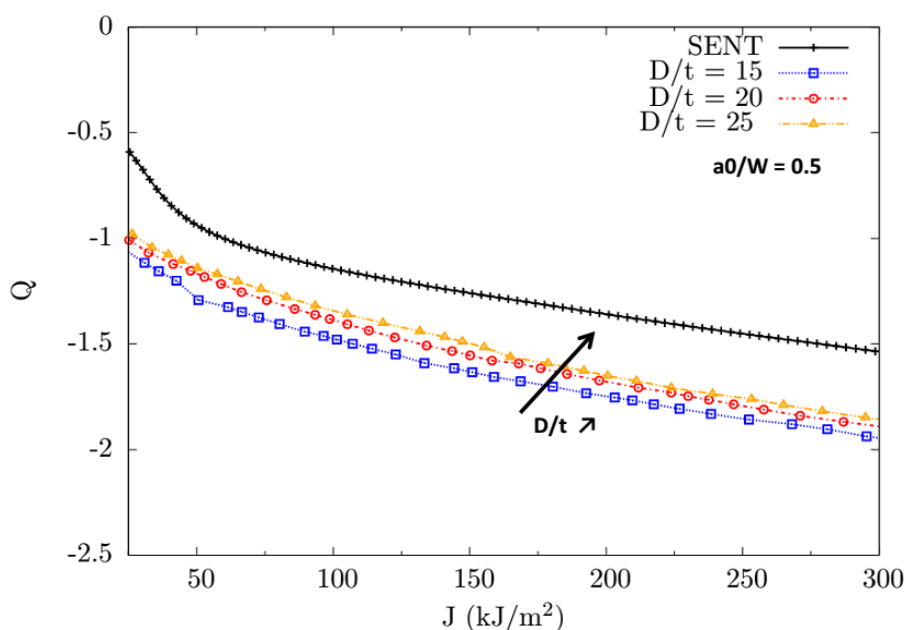


Figure 7 - Effect of the  $D/t$  ratio on the constraint  $Q$ . Comparison with the SENT specimen. ( $a_0/W = 0.5$ )

### 3. SENT TESTING

Zhu *et al.* [12] gave the outlines of the procedures from DNV, USP, ExxonMobil, CanMet, British Standard and UGent. From these, three main methods are identified: the multiple specimens method by DNV for  $J$ -R curve testing; the single specimen method developed by CanMet for  $J$ -R and CTOD-R curve ; and the single specimen method developed by ExxonMobil for CTOD-R curve.

#### 3.1 Specimen geometry and preparation

Specimen geometry and preparation are compared in table 1.

	DNV	ExxonMobil	CanMet
<b>Loading Condition</b>	Clamped, $H = 10 W$ or Pin-loaded	Clamped, $H = 10 W$	Clamped, $H = 10 W$

	<b>DNV</b>	<b>ExxonMobil</b>	<b>CanMet</b>
<b>Cross-Section</b>	$B = 2W$	$B = W$	$B = W$
<b>Initial crack length to thickness ratio <math>a_0/W</math></b>	0.2 – 0.5	0.25 – 0.35	0.05 – 0.95
<b>Crack preparation</b>	Fatigue pre-cracking in accordance with BS 7448.	Fatigue pre-cracking in accordance with ASTM E1820 or EDM notched with a wire diameter of 0.15 mm or smaller.	Fatigue pre-cracking in accordance with ASTM E1820
<b>Side-groove</b>	None	Total reduction of 10 % of the width with root radius of 0.5 mm (+/- 0.2 mm).	Total reduction of 10% of the width.

Table 1 - Geometry and preparation of the SENT specimens

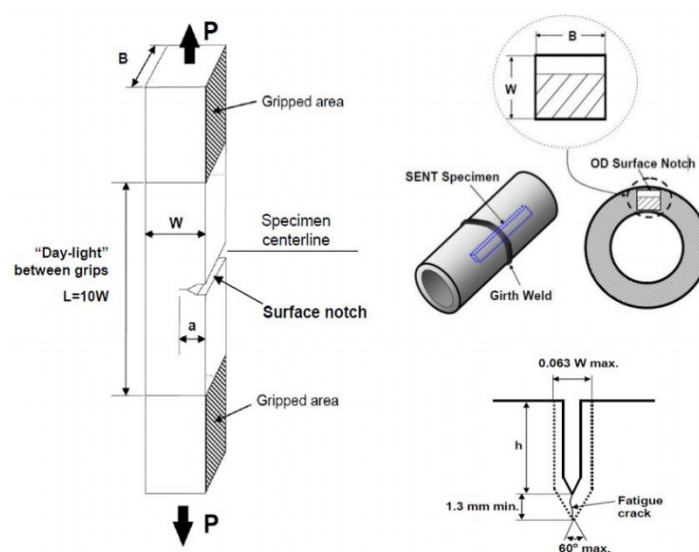


Figure 8 - Typical clamped SENT specimen [2]

When the fatigue pre-cracking procedure is advised in order to reach the targeted  $a_0/W$  ratio, it shall be done following BS 7448 or ASTM E1820 [5] recommendation for SENB specimen in 3-points bending cyclic loading, and before the side-grooves machining.

### 3.2 Testing conditions

The testing conditions for SENT tests are summarized in table 2.

	<b>DNV</b>	<b>ExxonMobil</b>	<b>CanMet</b>
<b>Type of approach</b>	Multi-specimens with a minimum of 6 valid specimens for R-curve.	Single-specimen with a minimum of 3 weld metal and 3 HAZ specimens	n.a.
<b>Tearing lengths</b>	0.2 – 3 mm	Not exceeding $0.2B_0$	No requirement
<b>R curve</b>	J-R curve or CTOD-R curve	CTOD-R curve	J-R curve or CTOD-R curve
<b><math>\Delta a</math> measurement</b>	Optical after completion of the test	Unloading compliance	Unloading compliance
<b>Instrumentation</b>	CMOD or CTOD with double-clip gage method	CTOD with double-clip gage method	CMOD

Table 2 - Testing conditions and measurements

### 3.3 Crack size and crack sharpness effect

DNV does not give strict recommendations about the initial crack-size-to-thickness ratio  $a_0/W$  for the assessment of cracked pipes. According to DNV, the R-curve is crack size-independent, as long as  $0.2 \leq a_0/W \leq 0.5$ . This conclusion is derived from a study by Nyhus *et al.* [13] where the effect of the crack depth on the ductile tearing resistance has been studied.

In particular, SENT tests have been performed on a 12" X65 parent material with three different  $a_0/W$  ratios (0.2, 0.35 and 0.5). The CTOD-R curves derived from these tests are depicted in Figure 9. One can see that for small value of tearing (approx.  $\leq 1$  mm), the CTOD-R curve is actually crack size independent. However, the curves seem to split for higher values. As an example, for a tearing value of 1.5mm, the difference for the CTOD values between  $a_0/W=0.25$  and  $a_0/W=0.5$  is approximately of 15%. An identical difference (about 15%) is shown in another study performed on a 13%Cr parent material for  $a_0/W=0.25$  and  $a_0/W=0.5$ . However, DNV recommendation for the maximum allowable crack extension being of 1mm, this difference may be not significant since only low values of tearing are considered.

Kang *et al.* [14] conducted a study on the constraint effect on the R-curve, and opposing results have been presented. A series of SENT tests have been performed on shallow ( $a_0/W=0.2$ ) and deep ( $a_0/W=0.5$ ) specimens. The specimens were prepared by fatigue pre-cracking and EDM. When comparing the R-curves (see Figure 10), one can clearly see that shallow specimens produce higher  $J$ -R curves when higher tearing values are considered. Also, it is shown that the preparation of the specimen only has a slight effect on the  $J$ -R curve, with EDM notch specimen producing slightly higher  $J$ -R curves.

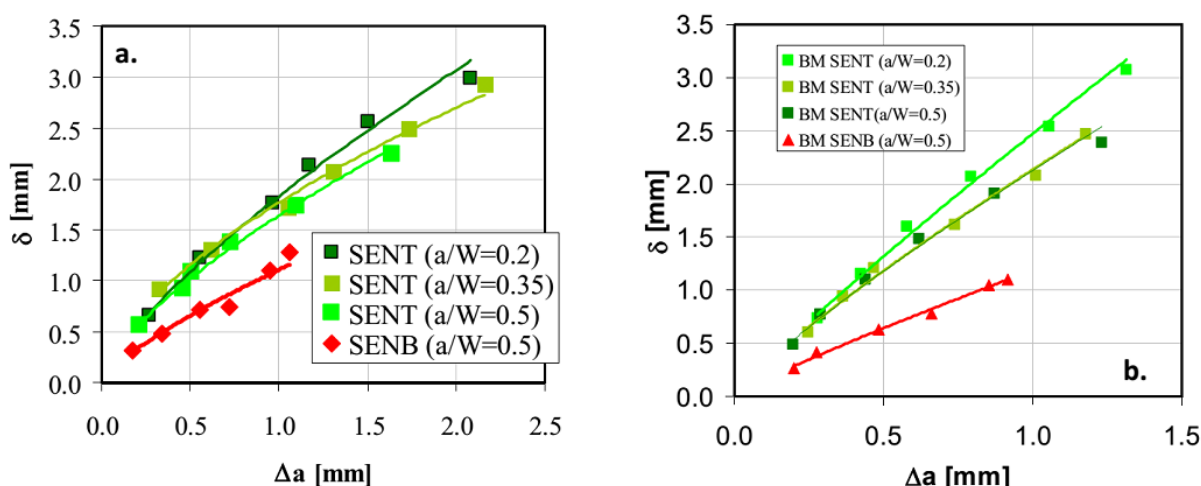


Figure 9 - CTOD-R curves obtained for different crack sizes on a 12" X65 parent material (a.) and a 12%Cr parent material (b.) [13]

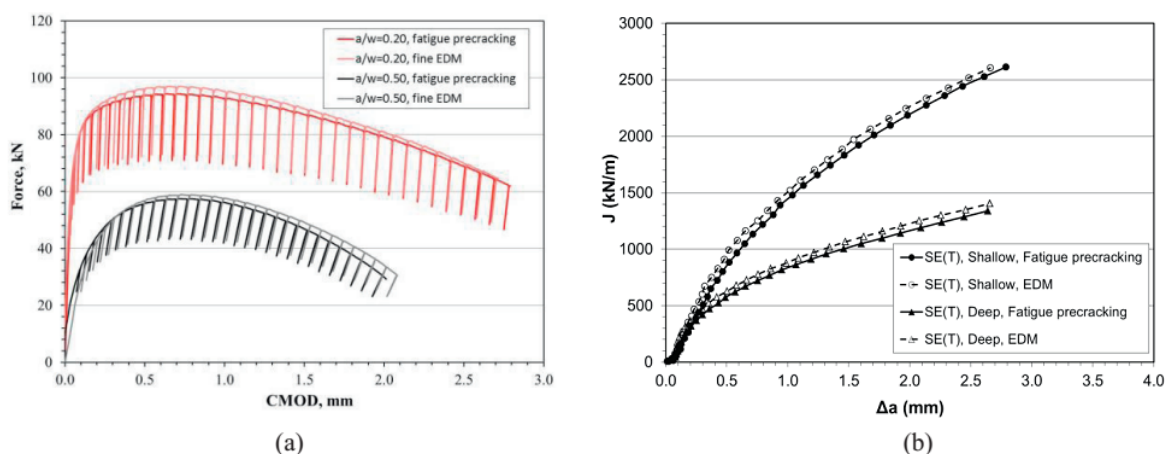


Figure 10 - Comparison of shallow notched ( $a_0/W=0.20$ ) and deep notched ( $a_0/W=0.5$ ) SENT specimens. Results for both fatigue pre-cracked and EDM notched specimens are given [14].

The main conclusions are:

- the  $a/W$  ratio may have influence on  $J$ - $R$  curves in particular for tearing larger than 0.8 mm. Based on existing experimental comparisons, the range proposed by ExxonMobil (0.25 – 0.35) seems to be the most relevant. For comparison, it is also of interest to remind that for workmanship type criteria,  $a_0/W$  are around 0.35 for onshore pipelines and around 0.15 for deepwater pipelines.
- at least for ductile material (see Kang [14] and Moore [15]), very similar results are obtained with fatigue pre-cracked and EDM notched specimens. Therefore, also for the test protocol selection, before using EDM notch SENT specimens, this is important to establish the Charpy transition curve to ensure the minimum pipeline design temperature is in the upper-shelf.

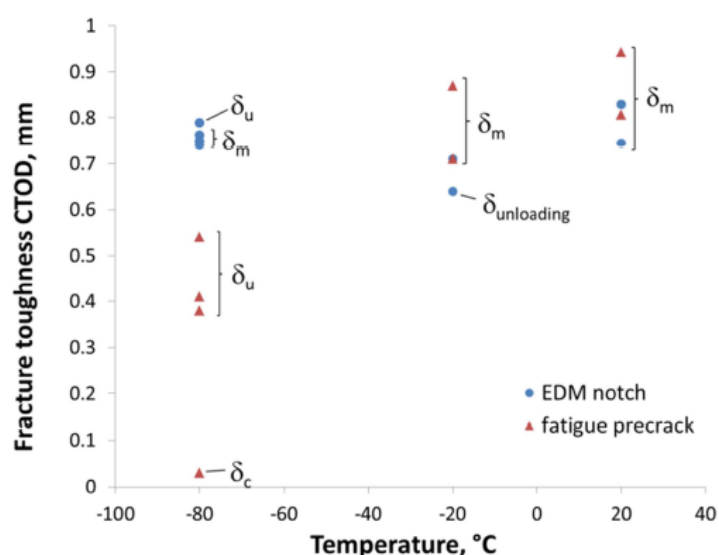


Figure 11 – Impact of EDM vs. fatigue pre-crack for brittle and ductile material (Moore [15])

### 3.4 $J$ vs. CTOD

There are different ways to measure the CTOD values as summarised in figure 12.

- $CTOD_5 = \delta_5$ : Opening measured between two points at the crack tip level over a 5 mm distance.
- $CTOD_{36}$ : Opening measured in the lips of the crack at 0.36 mm of the tip (this method is used by ExxonMobil to follow the CTOD in pipe finite element calculations).
- $CTOD_{tip}$ : Opening measured at the intersection between the lips and the 45° angle from the tip without taking the specimen deformation into account.
- $CTOD_{45}$ : is similar to  $CTOD_{tip}$  but the strain of the specimen is taken into account
- Double clip method: the principle is explained in Figure 12b.

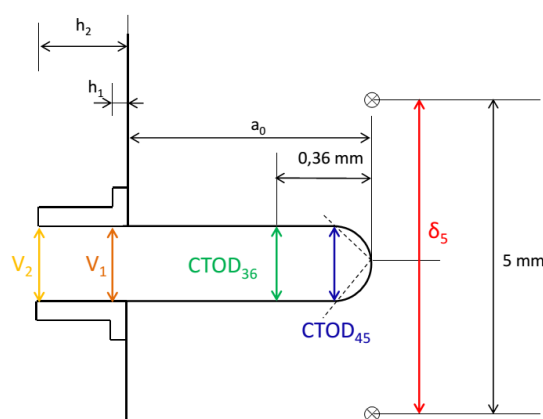
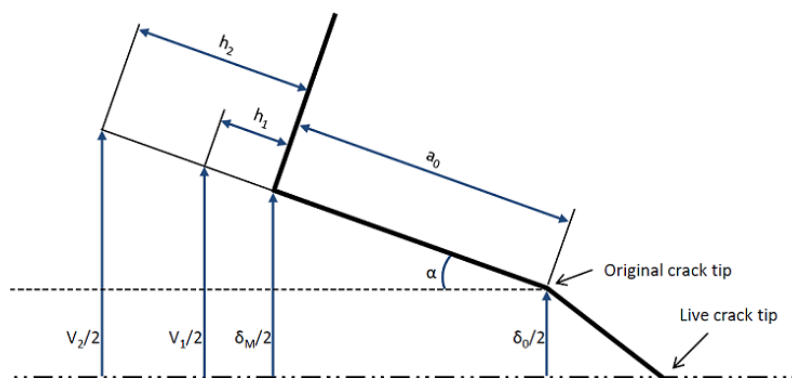


Figure 12a – Possible definition for CTOD



$$CTOD_{double-clip} = V_1 - \frac{a_0 + h_1}{h_2 - h_1} (V_2 - V_1)$$

Figure 13b – Double clip determination of CTOD

The below comparison (figure 13) has been performed based on 3D FE calculations on a SENT specimen ( $a_0/W = 0.25$ ). It shows that the five methods described above can lead to non negligible differences of the  $J$ -integral value for which the “same” CTOD.

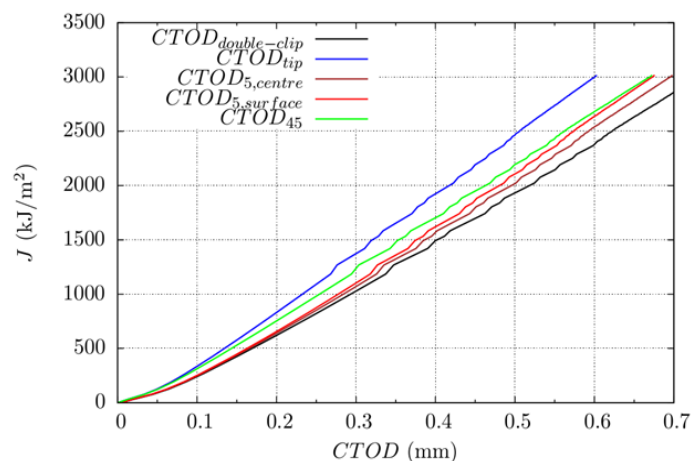


Figure 14 – J vs CTOD for various CTOD definitions

Moreover, some standards as the DNV OS F101 recommend not to measure the CTOD but to calculate the CTOD from the  $J$  value. As shown by (Moore, Pisarsky ...) the DNV approach is conservative whereas the double clip method might be non conservative especially for low  $a/W$  ratio.

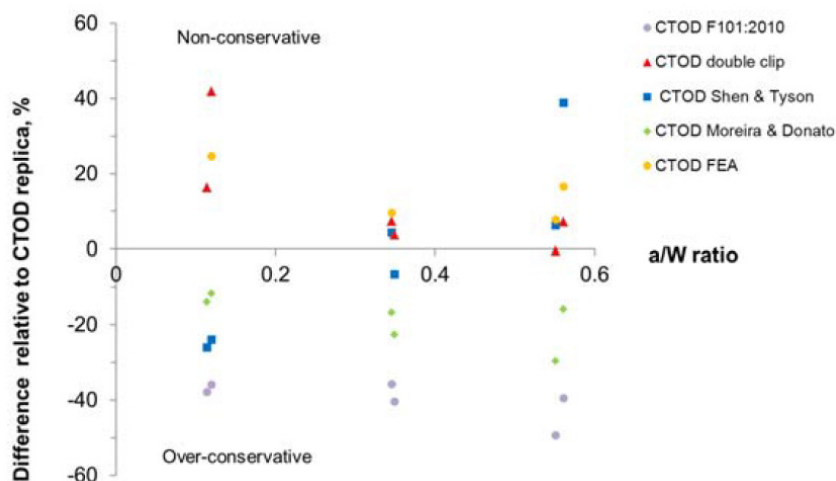


Figure 15 – Comparison of CTOD values and replica from Moore and Pisarsky [25]

The following conclusions can be raised:

- CTOD value is dependent from the measuring method. For assessment methods based on CTOD (like for ExxonMobil), it is important to either use the same reference for experiments and FE calculations or to account for the possible differences between the CTOD as measured experimentally and as “tracked” in FE calculations.
- When CTOD is directly determined from experiments, the CTOD value can be overestimated by 10%, 20% or more.

### 3.5 *J*-integral measurement

The plastic parameter  $\eta_p$  enables to calculate the plastic component of the *J*-integral from a normalized plastic energy value, using the following relationship:

$$J_p = \eta_p \frac{U_p}{B_N(W - a_0)} \quad (6)$$

where  $U_p$  is the plastic area under the load vs. CMOD,  $B_N$  is the net specimen thickness and  $W - a_0$  is the remaining ligament. This dimensionless parameter is geometry and loading dependent. (In the following, only clamped specimens are considered). Also, the values for CT and SENB specimens, which are normalized, do not apply. Different definitions for  $\eta_p$  have been found in the literature. In DNV-RP-F108, two equations are proposed (clamped and pin-loaded) for the calculation of  $\eta_p$  as a function of the crack length-to-thickness ratio  $a/W$  and the width-to-thickness ratio  $B/W$  (for  $1 \leq B/W \leq 5$ ). The expression for clamped specimens writes:

$$\begin{aligned} \eta_p = 0.85 \times \left\{ \left( 196.719 \cdot e^{-(B/w)} - 64.642 \right) \cdot \left( \frac{a}{W} \right)^5 + \left( -493.511 \cdot e^{-(B/w)} + 138.837 \right) \cdot \left( \frac{a}{W} \right)^4 \right. \\ \left. + \left( 463.503 \cdot e^{-(B/w)} - 106.207 \right) \cdot \left( \frac{a}{W} \right)^3 + \left( -201.862 \cdot e^{-(B/w)} + 34.532 \right) \right. \\ \left. \cdot \left( \frac{a}{W} \right)^2 + \left( 39.413 \cdot e^{-(B/w)} - 4.525 \right) \cdot \left( \frac{a}{W} \right) + \left( -2.064 \cdot e^{-(B/w)} + 1.039 \right) \right\} \quad (7) \end{aligned}$$

where the coefficient 0.85 is included in order to take into account work hardening and weld metal mismatch.

Cravero and Ruggieri [16] expression derives from a series of 3D finite elements analyses with the initial crack depth  $a_0$  within the range  $0.1 \leq a_0/W \leq 0.7$ . It writes:

$$\eta_{Cravero} = 1.0398 - 0.687 \left( \frac{a_0}{W} \right) \quad (8)$$

Finally, CanMet expression writes:

$$\begin{aligned} \eta_p = 1 - 1.089 \cdot \left( \frac{a}{W} \right) + 9.519 \cdot \left( \frac{a}{W} \right)^2 - 48.572 \cdot \left( \frac{a}{W} \right)^3 + 109.225 \cdot \left( \frac{a}{W} \right)^4 - 74.116 \cdot \left( \frac{a}{W} \right)^5 \\ - 77.984 \cdot \left( \frac{a}{W} \right)^6 + 38.487 \cdot \left( \frac{a}{W} \right)^7 + 101.401 \cdot \left( \frac{a}{W} \right)^8 + 43.306 \cdot \left( \frac{a}{W} \right)^9 \\ - 110.770 \cdot \left( \frac{a}{W} \right)^{10} \quad (9) \end{aligned}$$

In this study, a finite element analysis has been performed using the Abaqus FE code to compare CanMet, Cravero and DNV formulations. Two types of specimens have been considered: rectangular cross-section with  $B=2W$  and square cross-section with  $B=W$ . A typical mesh of a  $B=W$  specimen is shown in Figure 16 with elements of size  $50 \times 50 \mu\text{m}$  in the crack propagation direction and opening direction. An elastic-plastic law derived from an API-5L X65 steel was used. The *J* value has been extracted along ten integration contours in the width direction and a mean value of *J*, denoted  $J_{mean}$ , has been calculated using a weighted average method. The maximum *J* value, located at the mid-width of the specimen and denoted  $J_{max}$ , has also been extracted.

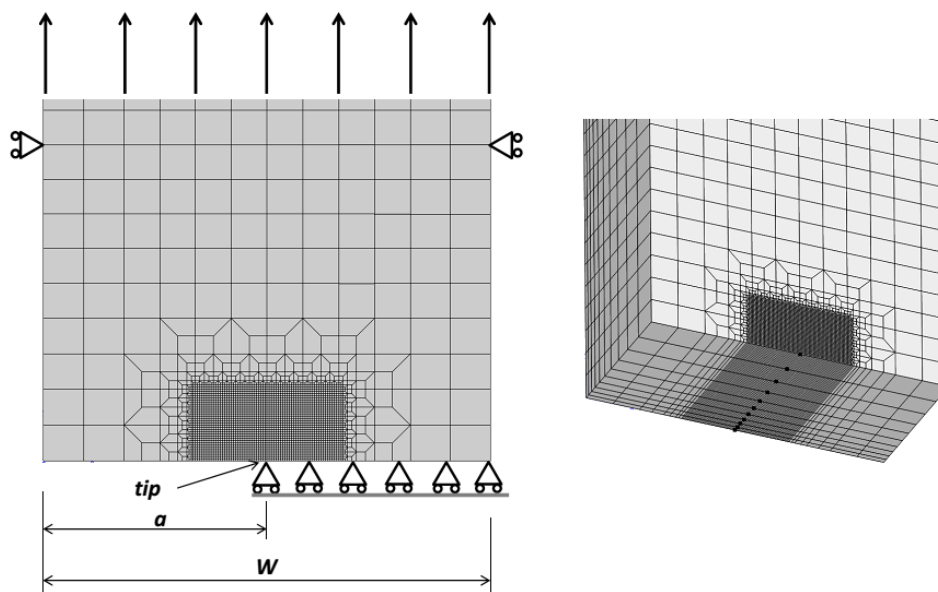


Figure 16 - 1/4 mesh of a BxB SENT for the calculation of  $J$  with Abaqus. In the refined area, the mesh size of 0.05x0.05mm.

The FEA results have been processed to get the CMOD-load plastic curve and the  $J$ -integral value for each time increment. Finally, the values of  $\eta_p$  by obtained by solving equation 6. In Figure 17, comparisons are made with equations 7, 8 and 9 where  $J$  has been taken as  $J_{mean}$ . As one can see, CanMet and Cravero formulations fit the numerical results with a good accuracy for all the specimens ( $B=W$  and  $B=2W$ ) over the all range of validity. However, the DNV curves do not fit well the numerical results, in particular for squared cross-section specimens.

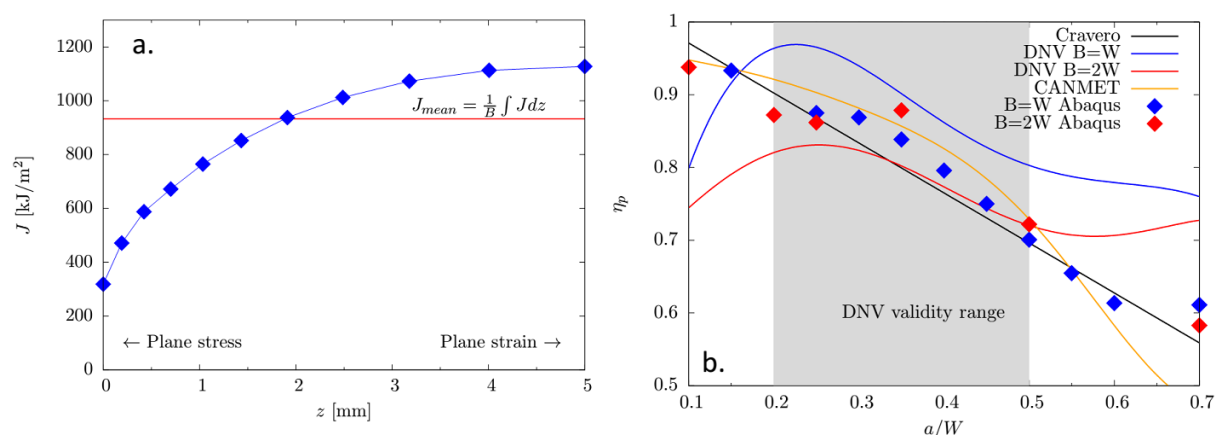


Figure 17 - On the left: Variation of the  $J$  value through the width of the specimen. Comparisons between analytical and numerical results for  $J=J_{moy}$ .

Other comparisons are made in Figure 18 where the  $J$  extraded from FEA has been taken equal to  $J_{max}$ . In Figure 18a., the analytical curves from DNV-RP-F108 are plotted with the “safety” factor 0.85 applied (see equation 7). It results in the solid lines colored in blue ( $B=W$ ) and red ( $B=2W$ ). An identical comparison is made in Figure 18.b where the safety factor has not been taken into account, resulting in higher DNV curves (solid lines colored in blue and red). As one can see, the DNV curves fit the numerical values with a very good accuracy.

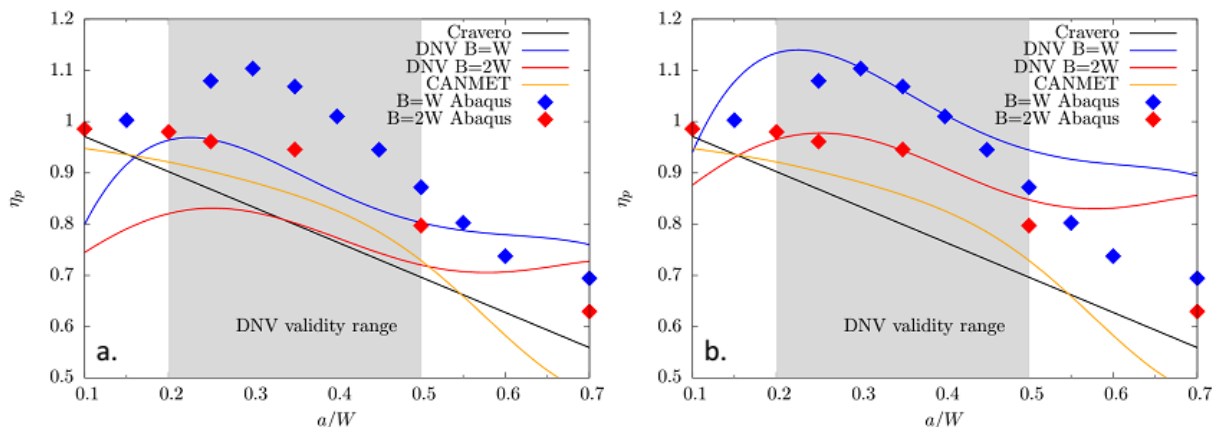


Figure 18 - Comparisons between analytical and numerical results for  $J=J_{moy}$ . In plot a., the margin factor 0.85 is applied, whereas plot b. shows the results without the margin factor.

These numerical results point out the question on how the  $J$ -integral value should be calculated when FEA is used. Indeed, the use of  $J_{max}$  instead of  $J_{mean}$  will conduct to under conservative  $J$ -R curves as one can see in Figure 19 where  $J$ -CMOD curve are plotted for  $B=W$  and  $B=2W$  SENT specimens ( $a_0/W=0.5$ ). This phenomenon is more significant for  $B=W$  specimens where the region under plane strain conditions, where  $J$  is maximum, is limited across the width.

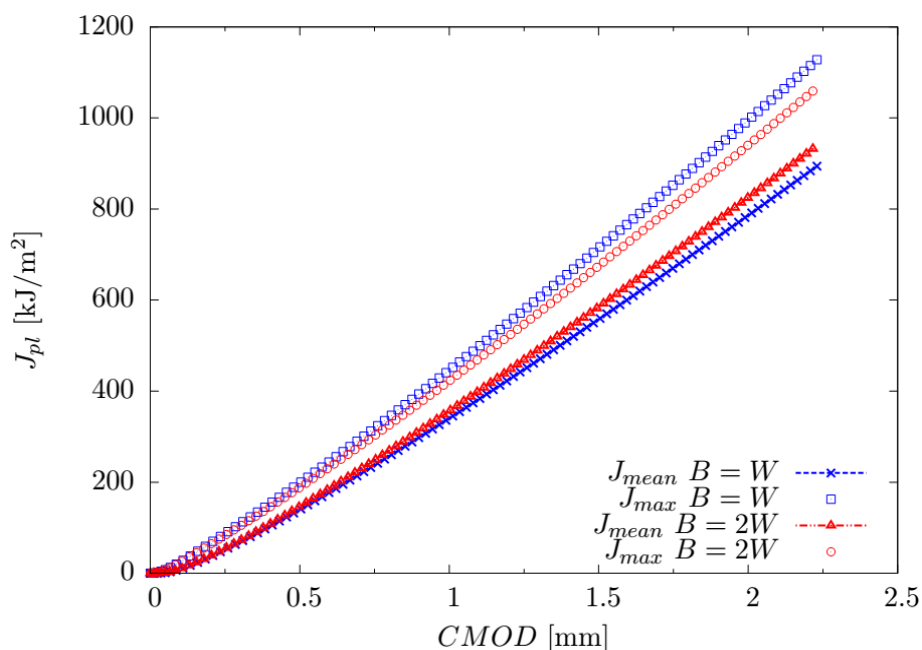


Figure 19 - Evolution of  $J_{max}$  and  $J_{mean}$  as a function of the CMOD for  $B=W$  and  $B=2W$  SENT specimens. ( $W=10\text{mm}$  and  $a_0/W=0.5$ )

#### 4. THE FAD APPROACH

##### 4.1 FAD and strain based design

The use of FAD in strain based design requires the “translation” of the applied strain level into an “equivalent” stress which by essence exceeds the material yield strength. The approach given in RP-F108 is as described in Figure 20.

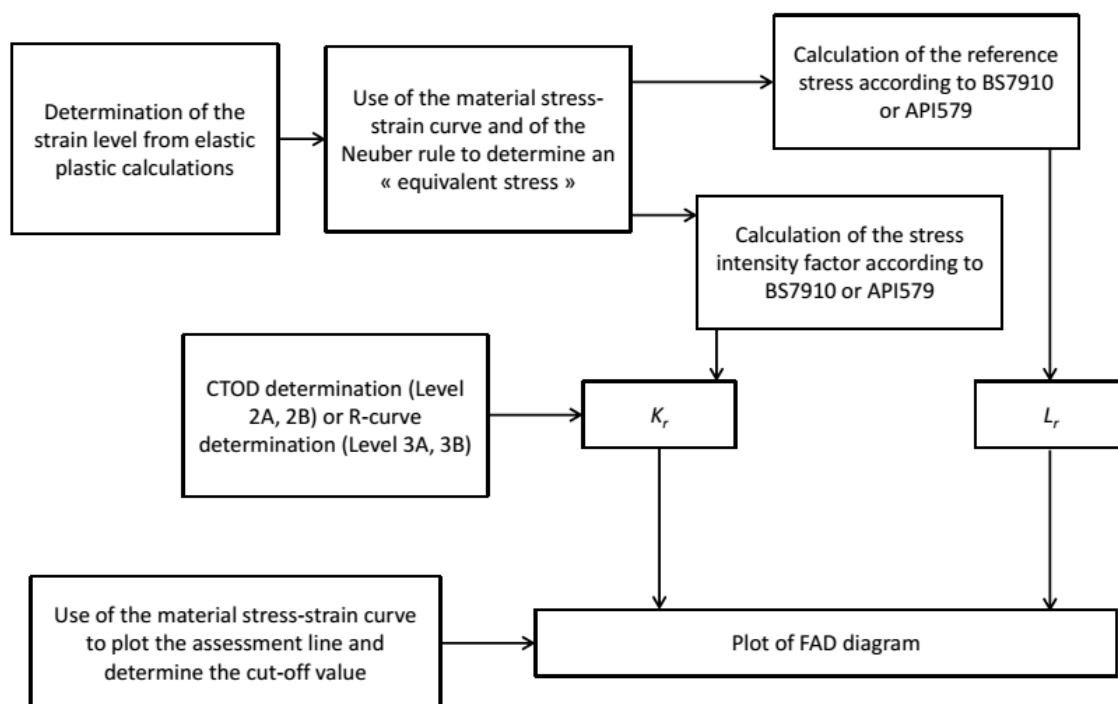


Figure 20 - FAD approach

## 4.2 Points of discussions around the FAD approach

Some points of discussions are the same for stress and strain based design approaches:

- How to account for biaxial loading? FAD is based on the opening stress. Therefore, the two ways to account for biaxial loading are either to add a correction to the uniaxial stress or the revisit stress intensity and reference stresses calculations (the first way being the easiest one).
- How much conservative is the reference stress calculation for embedded defects? The difficulty with embedded defects is that the failure occurs in two steps: the failure of the ligament and then the through wall failure. DNV has recently recommended the use of the same acceptance criteria than for surface breaking defects whereas BS 7910 recommends to assess the embedded defect and then the surface breaking defect where the defect depth includes the ligament.

For strain based design the reference stress and the assessment line in the cut-off region are obviously key parameters as strain based design “explores” the right bottom side of the failure assessment diagram.

## 5. THE TANGENCY ANALYSIS

### 5.1 Principle

The principle of the tangency approach is described in Figure 21. It is based on the fact that the history of the crack, *i.e.* the plasticity developed around the crack tip during the loading, does not modify the driving force. It means that a driving force (CTOD- $\Delta a$  or  $J\Delta a$ ) can be directly obtained by a series of FEA simulations for stationary cracks with a growing  $a_0/W$  ratio. Then, the CTOD or  $J$  value is extracted from each numerical simulation, *i.e.* for each crack growth, as a function of the applied remote strain, and iso-strain driving forces are plotted. In Figure 21, three driving forces are plotted for three strain levels ( $\varepsilon_1 < \varepsilon_2 < \varepsilon_3$ ).

This approach simplifies the numerical work, since it does not require the use of complex damage model to simulate the crack propagation during the simulation.

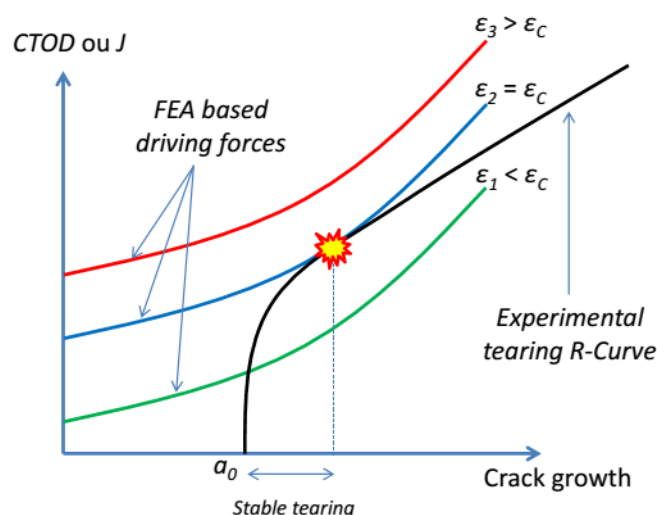


Figure 21 - Principle of the tangency analysis

## 5.2 The 3D J-integral determination

When the driving forces are expressed in terms of  $J$  values, the question of its definition and calculation by means of FEA should be raised.

It has been seen hereinbefore that for a straight crack front, the value of  $J$  depends on the position of the measurement point along the crack front. At the centre of the crack, where plane strain conditions exist, the  $J$  value is maximum. On the contrary, at the free surfaces, where plane stress conditions exist, the  $J$  value is minimum (see Figure 1716). We have seen that a mean  $J$  value may be defined by integrating  $J$  along the crack front. This definition may be more physical since the entire crack front contributes to the energy release during the tearing process.

In a real-world assessment, crack does not have a straight crack front and may be considered as a semi-elliptical crack. Such a crack does not propagate uniformly along the front, but generally grows in the wall thickness direction first before growing in the circumferential or longitudinal direction [17]. In such a case, it may be relevant to consider the  $J$  value measured at the centre of the crack.

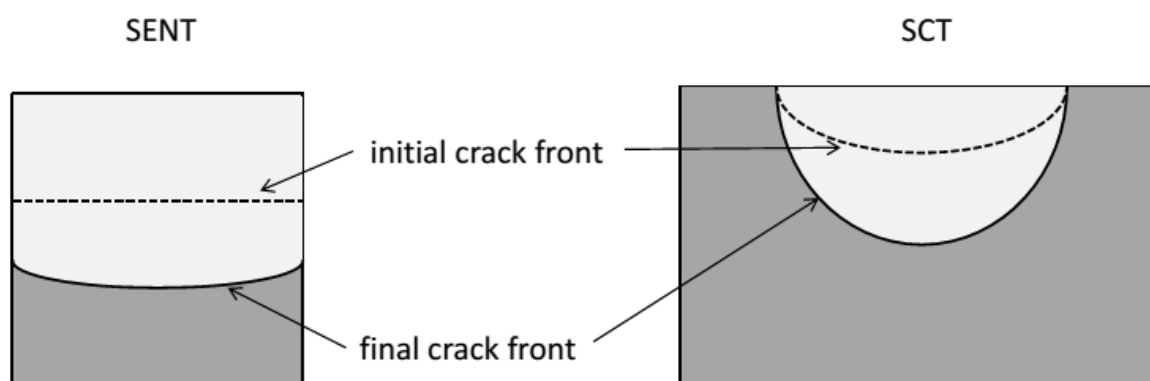


Figure 22 - Schematics of a crack propagation depending on the initial shape of the crack. (Single Edge Notched Tensile specimen and Surface Crack Tensile specimen).

The calculation of  $K$ -factor or  $J$  value in a three dimensional structure by means of FEA is not straightforward for cracks with non-straight crack front, such as semi-elliptical cracks. In this study, a comparison has been made between FE calculated and reference  $K$ -factors from Newman-Raju [18].

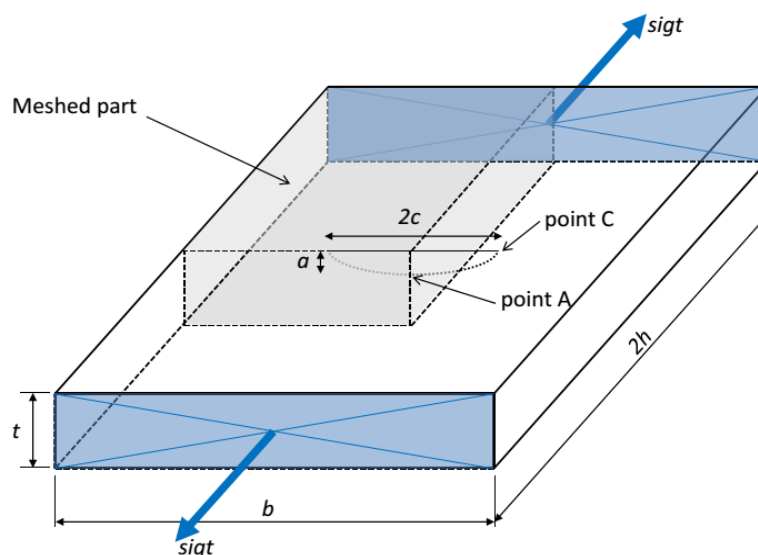


Figure 23 - Surface Crack Tensile specimen geometry

The numerical study has been conducted using Abaqus finite element software. A SCT specimen has been considered with the geometry as depicted in Figure 24 where  $t = 10\text{mm}$ ,  $b = 20\text{mm}$ ,  $a = 6\text{mm}$  and  $c = 12\text{mm}$ . 5.3

The mesh consisted in 73,248 3D linear elements (eight nodes) using full integration (C3D8) with small scale formulation. An elastic steel with a Young's modulus  $E=205\,000\text{ MPa}$  and a Poisson's ratio  $\nu=0.33$  has been defined, and  $J$ -integral values and  $K$ -factor values have been extracted using the Abaqus built-in function "cracks" at points A and C (see Figure 25) with taking care of choosing integration contours where the convergence was achieved.

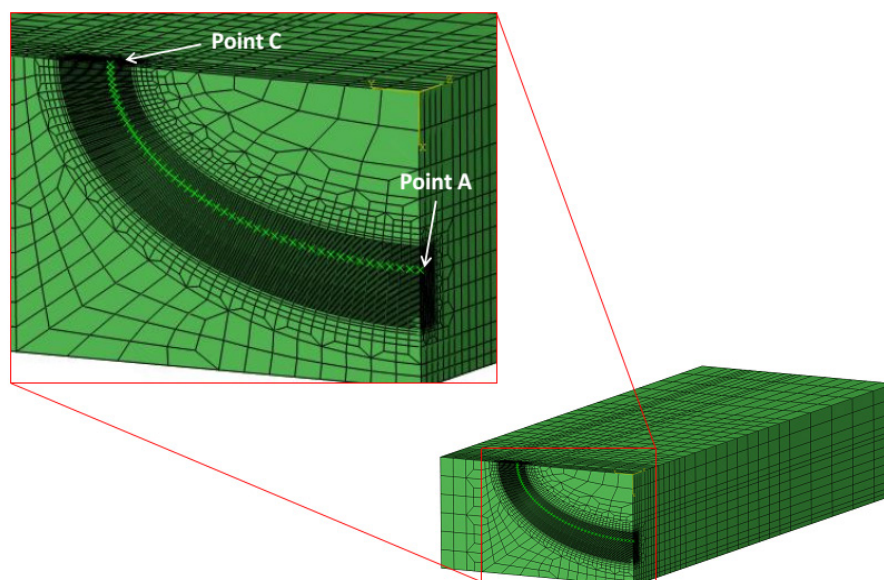


Figure 24 - 3D mesh of the SCT specimen in Abaqus for the validation of the stress intensity calculation

Point	$K_I$ reference	$K_{I,Abaqus}$	% error on $K_I$	% error on $J_e$
A	5.4009	5.0460	6.57 %	13.14%
C	4.6822	4.6748	0.15 %	0.30%

Table 3. Comparison between reference SIF from Newman and Raju [18] and calculated SIF using Abaqus.

As one can see in Table 3, the  $K_{I,Abaqus}$  underestimates the reference solutions at point A by 6.57%, respectively at C point by 0.15%.

The elastic part of the  $J$ -integral is directly derived from the  $K$  value using the relationship  $J_e = K^2/E'$  where  $E' = E$  in plane stress conditions and  $E' = E/(1 - \nu^2)$  in plane strain conditions. It is rewritten to obtain the derivative of  $J_e$  as a function of the derivative of  $K$ , which gives  $dJ_e/J_e = 2 dK/K$ . It means that the  $J$ -value is underestimated by 13.14% at point A, and of 0.30% at point C. This result must be investigated since it may lead to under-conservative driving force if used in the tangency analysis. Further simulation with elastic-plastic material will be performed in order to check the validity of the plastic part of  $J$ ,  $J_p$ , which is predominant in strain-based approaches.

#### 5.4 Discussions around the determination of the crack driving force

The tangency approach is questionable as it has been pointed out by Rice and Ostby [20]. Such a dependency between plasticity and crack driving force curve only applies when the material is considered as non-linear elastic. However, in the case of elastic-plastic materials where the crack driving force curves stem from the plastic deformation in the crack ligament, it does not apply anymore.

The effect is explained in Figure 25. As one can see, the correction proposed by Ostby produces lower driving forces. In this figure, the driving forces as obtained by a classical tangency analysis method are depicted in solid lines, whereas the corrected driving forces are plotted in dashed lines. Therefore, it implies:

- for an existing flaw with a given crack depth, the critical strain  $\epsilon_c$  is higher;
- for a load given as a strain value, the critical initial crack depth  $a_{0c}$  is higher.

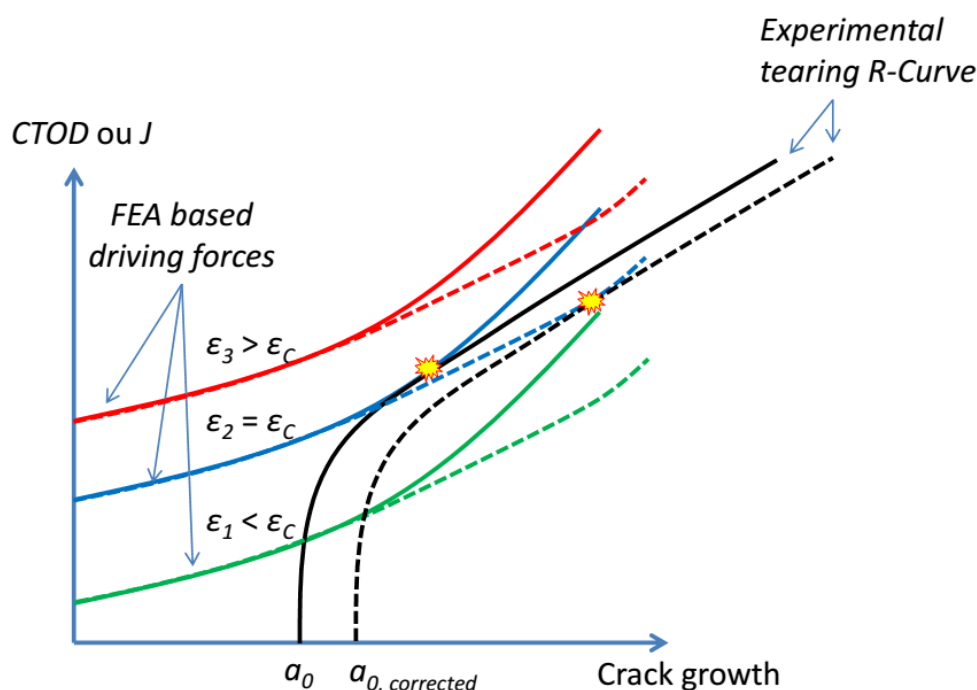


Figure 25 - Correction of the driving force curves as proposed by Ostby in order to take the plasticity at the crack tip vicinity into account.

#### 5.5 Discussions around the R-curve

The principle is to use the R-curve experimentally determined and then offset the curve to the desired  $a_0$  value. It means that the tangency analysis approach neglects the effect of the  $a_0/W$  ratio. As discussed in section 3.3, the  $a/W$  ratio may have a non negligible impact on the R-curve.

#### 5.6 Discussions around $J$ versus CTOD in the tangency approach

The R-curve used in the tangency analysis is determined from SENT tests. The crack driving force is determined by FE calculations.

To avoid any discussions around the determination of the  $J$ -integral, ExxonMobil has chosen to consider the CTOD- $\Delta a$  curve. This proposal is supported by experimental work.

However to ensure transferability from the pipe to the SENT specimens it has been evidenced by ExxonMobil that the SENT test must be performed with an  $a_0/W$  ratio of 0.1 less than the  $a_0/W$  ratio on the pipe. Following this recommendation and considering that for the SENT test  $0.25 \leq a_0/W \leq 0.35$ , the initial crack depth  $a_0$  within the pipe shall be in the range  $0.15 \leq a_0/W \leq 0.25$ . The range of applicable defect depth vs. pipe wall thicknesses is shown in Figure 26.

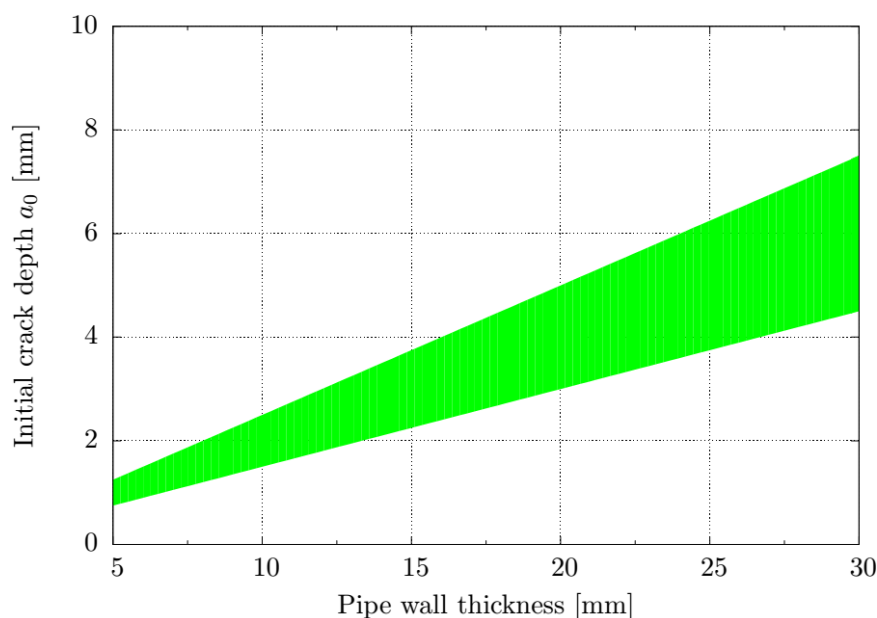


Figure 26 - Initial crack depth range as a function of the wall thickness according to ExxonMobil requirements

In addition, the CTOD approaches raise the question of the extraction of CTOD values from finite elements calculations.

## 6. LOCAL APPROACH TO DUCTILE FRACTURE

### 6.1 Principle

Ductile fracture is the result of three successive stages: void nucleation, growth and coalescence. In general, these phenomena appear at inclusions due to the strain incompatibility between the hard particles and the softer matrix. Since it is impracticable to model every void in a structure, many porous material models have been developed. One of the most common models is the so-called GTN model, developed by Gurson and later modified by Tvegaard and Needleman.

The methodology for the use of the local approach is described in Figure 27. It rests on the idea that a geometrical independent model is able to represent the local behaviour of the material. To do so, laboratory tests are performed in small scale specimen, and the inverse method is used in order to characterize the material in terms of both elastic-plastic behaviour and fracture mechanics. Then, some laboratory tests on specimen with plastic constraint condition close to the actual structure which is assessed are performed, and results are compared with FEA results realized using the previously identified models. If results fulfill any acceptance criterion, then the actual structure is meshed and FEA are performed.

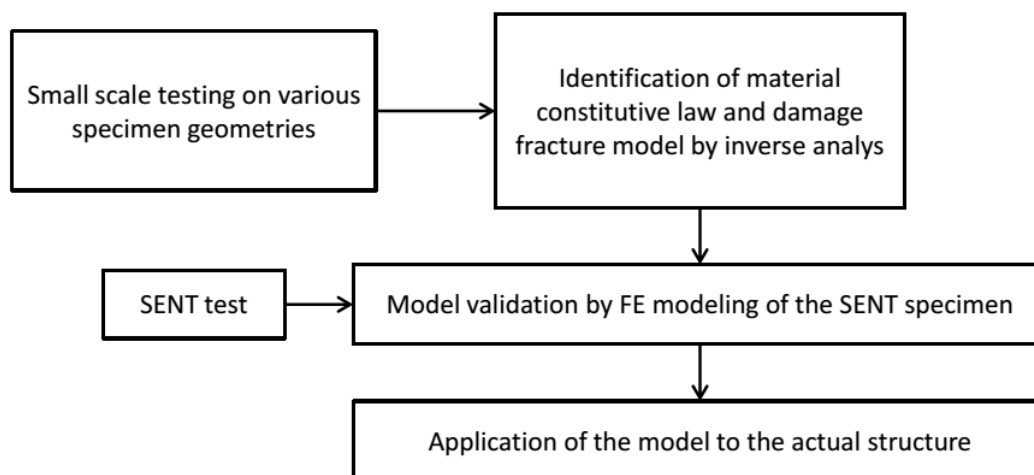


Figure 27 - Principle of the local approach to ductile fracture

## 6.2 Points of discussion

The main point of discussion with the local approach is that mesh size is a model parameter which may have to be adjusted at the model validation stage on SENT specimens.

On the material side, mesh size should be related to the grain size provided the grain is the relevant scale for fracture.

## 7. USE OF THE SENT IN ECA

### 7.1 Overview

Method	Material testing	Transferability	Assessment
DNV	SENT $B=2W$ $0.2 \leq a/W \leq 0.5$	Effective	BS 7910
ExxonMobil	SENT $B=W$ $0.25 \leq a/W \leq 0.35$	$(a_0/W)_{SENT} = (a_0/W)_{PIPE} + 0.1$	Analytic expression and tangency analysis using FEA
CanMet	SENT $B=W$	<i>n.a.</i>	<i>n.a.</i>
PRCI	Depending on assessment level	<i>n.a.</i>	Analytic expression and tangency analysis using FEA

Table 4 - Overview of the existing ECA based on the use of the SENT specimen

ExxonMobil suggests that the initial crack depth  $a_0$  must be in the range  $0.25 \leq a_0/W \leq 0.35$ .

### 7.2 Application

An outer surface semi-elliptical crack has been implemented by means of a grinder at the weld centreline of an API 5L-X65 seamless pipe. The geometry of the crack is defined in Figure 28. The initial crack length is  $2C = 65\text{mm}$ , the initial crack depth is  $a = 4\text{mm}$  and the initial crack thickness is about  $200\ \mu\text{m}$ .

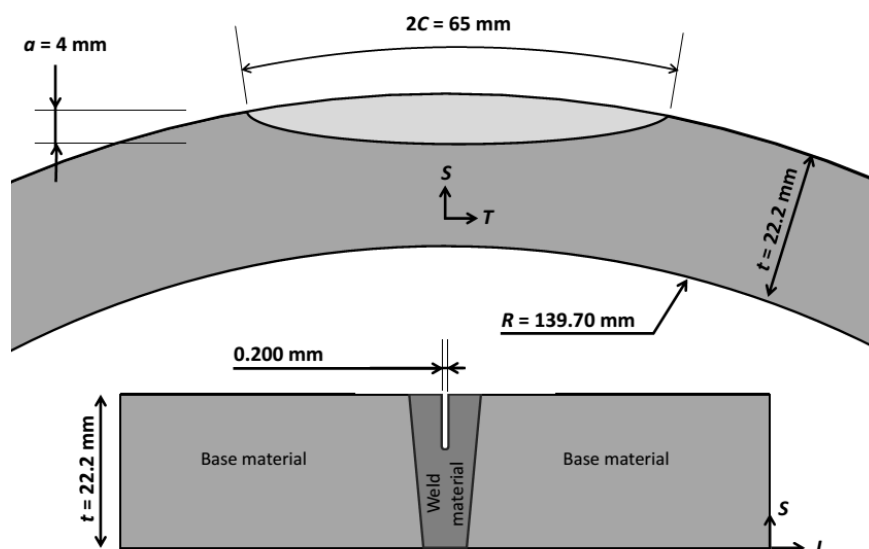


Figure 28 - Surface crack at the weld centreline with  $2C = 65$  mm and  $a = 4$  mm.

### 7.3 Test material and experimental procedure

A comprehensive characterization of the mechanical properties of base and weld materials was conducted. It ensured to perform all the ECA with actual materials characteristics, and allowed performing comparisons between simplified and advanced ECA. The identifications have been carried out using the inverse identification method by means of finite elements analysis with the software Z-Set. In the following, the longitudinal direction is referred to as “L”; the transverse (circumferential) direction is referred to as “T” and the short transverse (thickness) direction is referred to as “S”, as defined in Figure 29.

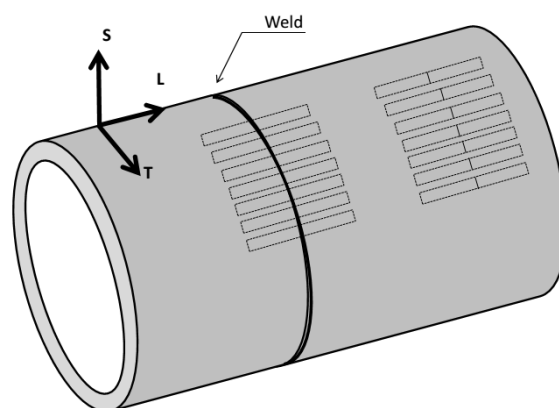


Figure 29 - Schematic diagram of pipe directions

Various specimens geometries as described in Figure 30 have been tested:

- NT2, NT4 and NT10 specimens allowed testing various stress triaxiality levels as this parameter is known to be a driving parameter in ductile fracture.
- DP specimens allowed testing the material in plane strain conditions which are deemed similar to loading conditions for pipeline with high  $D/t$  ratio.

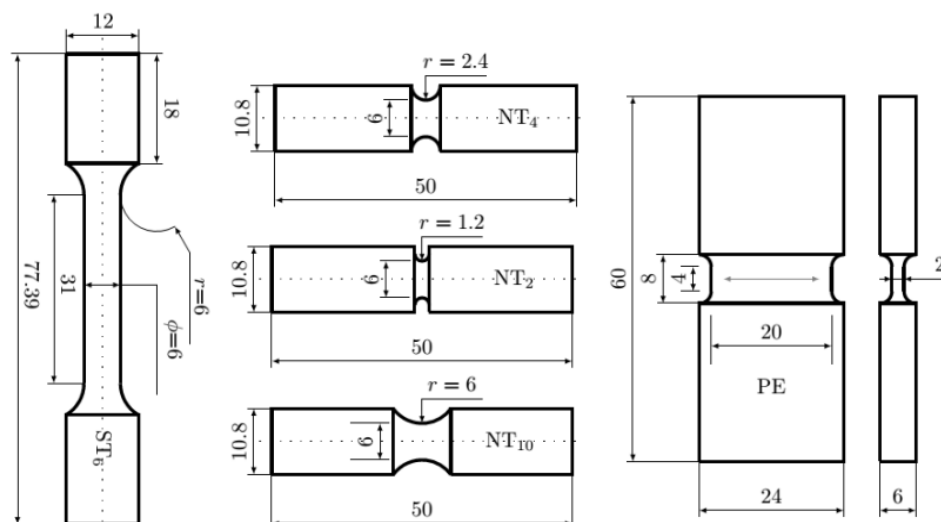


Figure 30 - Test specimens for base material characterization: ST: smooth tensile bar, NT = 2, 4, 10: axisymmetric notched tensile bars, PE: plane strain specimens where the plain strain direction is depicted with the thin grey line.

The base material has been tested along directions “L” and “T”, and the weld material has been tested only in the “L” direction which is the relevant direction in the case of a pipe loaded in tensile.

### 7.3.1 Base material flow curve

All tests were performed at room temperature on a servo-hydraulic testing machine under displacement controlled loading conditions. Test specimens include smooth tensile bars (ST), axisymmetric notched tensile bars ( $NT_x$ ) and plane strain specimens (PE). The traction tests on smooth tensile bars have been performed measuring the applied load  $P$ , gauge length elongation  $\Delta L$  and diameter reduction  $\Delta\emptyset$ . Tensile tests on axisymmetric notched tensile bars have been performed measuring the applied load  $P$ , the overall length elongation and the minimum diameter reduction  $\Delta\emptyset$ . Tensile tests on plane strain specimens have been performed measuring the applied load  $P$ , the overall length elongation, and DIC was used to measure the strain field within the minimum thickness region.

The yield stress was about 450 MPa and the ultimate tensile strength was about 550 MPa. The stress-strain curve displayed a Lüder's plateau of about 1% strain 1% to 1.5% strain (see Figure 31).

### 7.3.2 Weld material flow curve

Tensile specimens ( $ST_6$ ) have been used in order to determine the weld mismatch by means of DIC. However, it is not possible to obtain a full stress-strain curve of the weld material because the deformations are confined in the “softer” material, *i.e.* the base material. Therefore, notched tensile specimens were machined so that the weld material was located inside the notch. Then, it was possible to obtain a full stress-strain curve even beyond the ultimate strength up to failure. However, an inverse identification by means of FEA is required. Also, chemical attacks with 4% Nital solution (alcohol and nitric acid) were made on each specimen to ensure the positioning of the weld in the specimens.

The yield stress was about 534 MPa and the ultimate tensile strength was about 670 MPa. No Lüder's plateau was observed (see Figure 31).

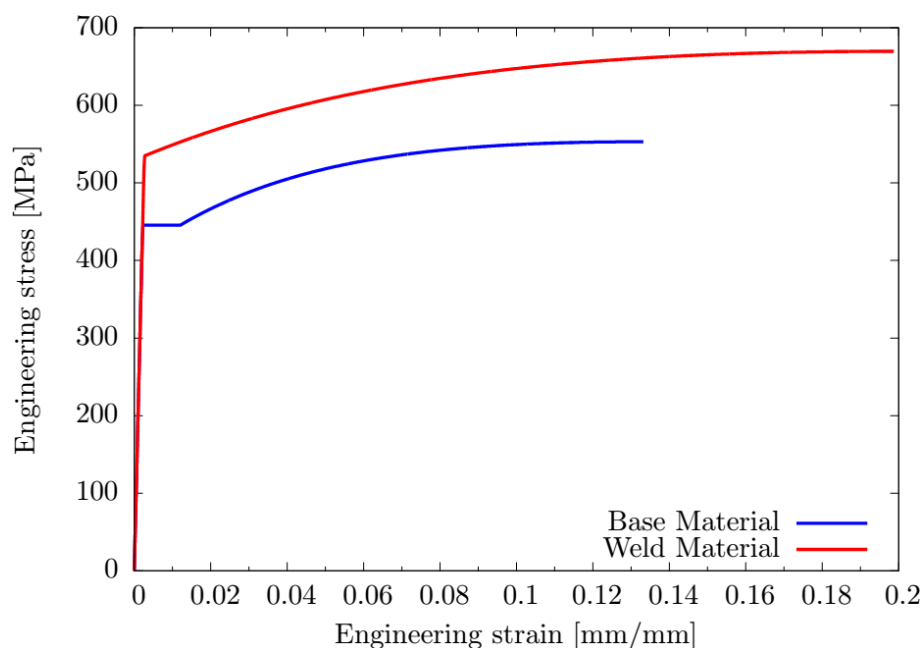


Figure 31. Engineering stress-strain curves of the parent material (API 5L X65) and the weld material.

## 7.4 SENT tests

### 7.4.1 Testing conditions

The SENT specimens were machined following ExxonMobil recommendations with a squared cross-section of 14x14mm, and side-groove equal to 10% of the thickness ( $B_N=12.6\text{mm}$ ). The specimen dimensions were deliberately reduced so the specimens could be tested on the laboratory facility.

For the base material characterization, the specimens were taken out from the pipe at the mid thickness far enough from the girth weld. For the weld metal characterization, the specimens were taken out at the mid thickness of the pipe and notched at the weld centerline.

The specimen were clamped using hydraulic grips with a distance between grips  $H$  equal to  $10W$ , as depicted in Figure 32. The initial notch was implemented using EDM method, with a  $\varnothing 300\mu\text{m}$  wire for the first 2.3mm and a  $\varnothing 100\mu\text{m}$  wire to reach an initial crack length of 3.5mm. Also, specimens have been prepared with a notch machined with a  $\varnothing 300\mu\text{m}$  wire only on the full length of the crack, with no further preparation before testing. This was made to study the effect of the notch sharpness with highly blunted crack. In both cases, it resulted in a  $a_0/W$  ratio of 0.25. The double clip gage method was used to measure both CMOD and CTOD, and unload/load cycles were performed with a maximum interval between each cycles of  $0.01W$  measured from the lower clip so that a complete CTOD-R curve was obtained.

Resulting curves are depicted in Figure 33 and Figure 34. As one can see in Figure 33, the R-curves obtained using the two different preparation procedures produce identical R-curves. Also, it appears that even widely blunted specimens can be used to characterize the material toughness of the material. However, further analyses shall be conducted on other material to confirm this result, since it may apply only on the case of ductile materials on the upper shelf of the ductile-brittle transition curve.

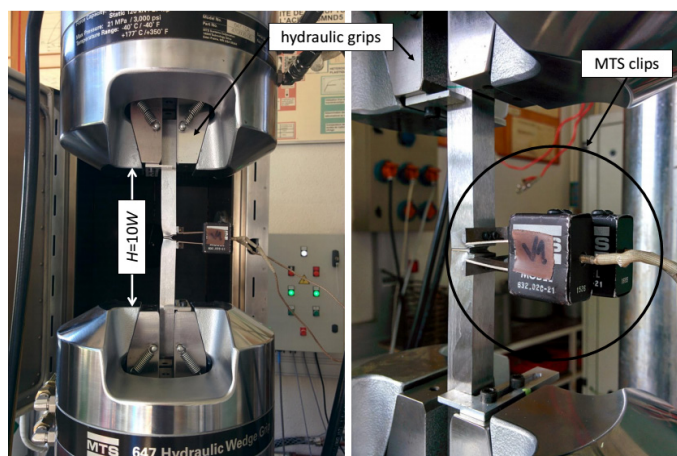


Figure 32 - Setup of SENT specimens with hydraulic grips, and double-clip gauges to monitor the CMOD and CTOD.

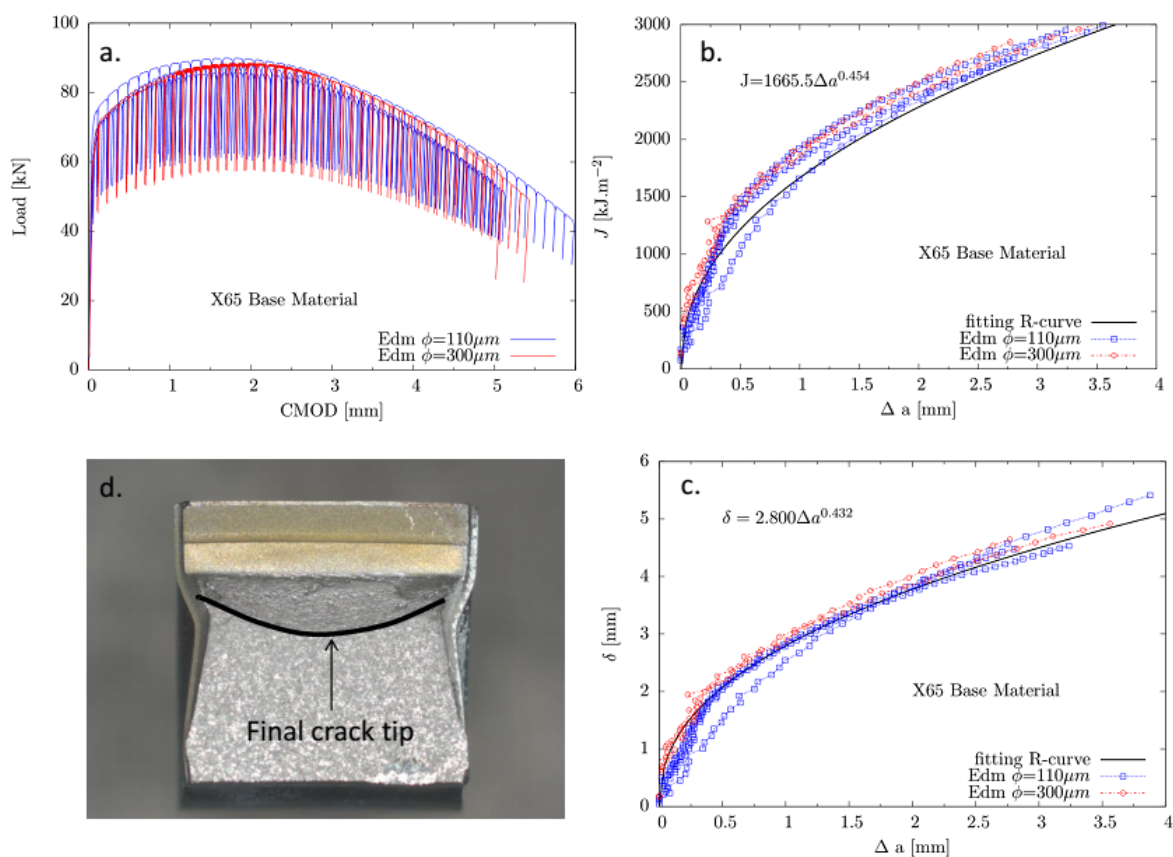


Figure 33 - CMOD-Load curve obtained from 3 SENT tests on the X65 base material (a).  $J$ -R curve (b) and CTOD-R curves (c) have been derived from these tests and fitted using a power law formulation. Specimens were broken after the tests using liquid nitrogen in order to measure the final crack length (d).

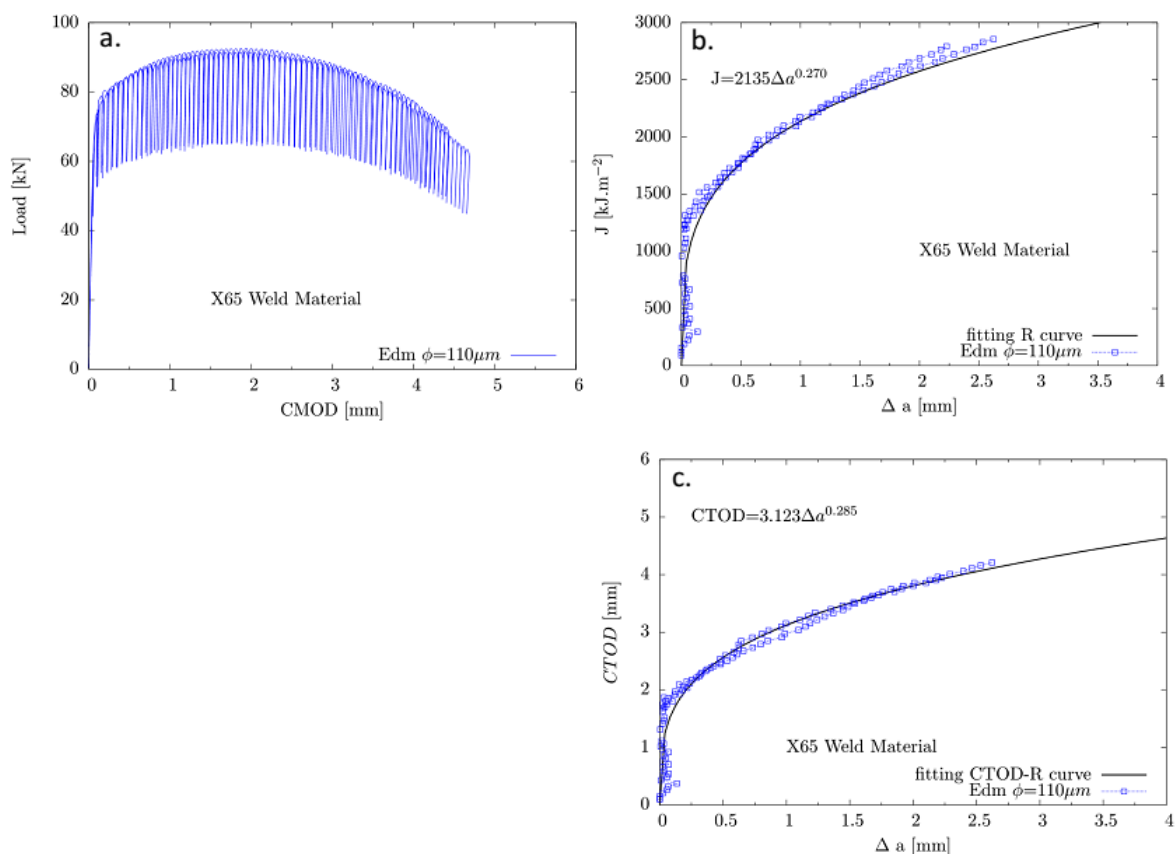


Figure 34 - CMOD-Load curve obtained from 3 SENT tests on the X65 weld material (a).  $J$ -R curve (b) and CTOD-R curves (c) have been derived from these tests and fitted using a power law formulation.

In addition the compliance method to generate a R-curve from one experiment has been validated by comparison with replica (see. Figure 35).

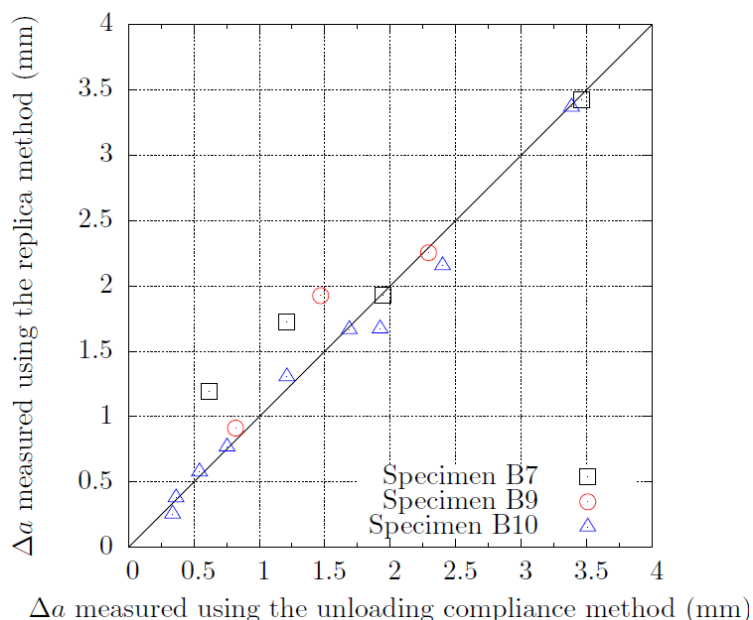


Figure 35 – Comparison between the unloading compliance method and the replica method

## 7.5 FAD approach

The FAD approach has used to assess the structure with the modifications as advised in DNV-RP-F108 for the extension of the approach to the strain-based design. (see section 4). Here, the aim is to determine the critical strain for the considered crack. Level assessment 3B from BS7910:2005 has been used, which corresponds to a ductile tearing assessment with the actual material properties.

The BS7910 level 3B FAD analysis results are shown in Figure 36. The predicted strain at the onset of pipe failure is around 5.3% with a crack opening of 1.5 mm.

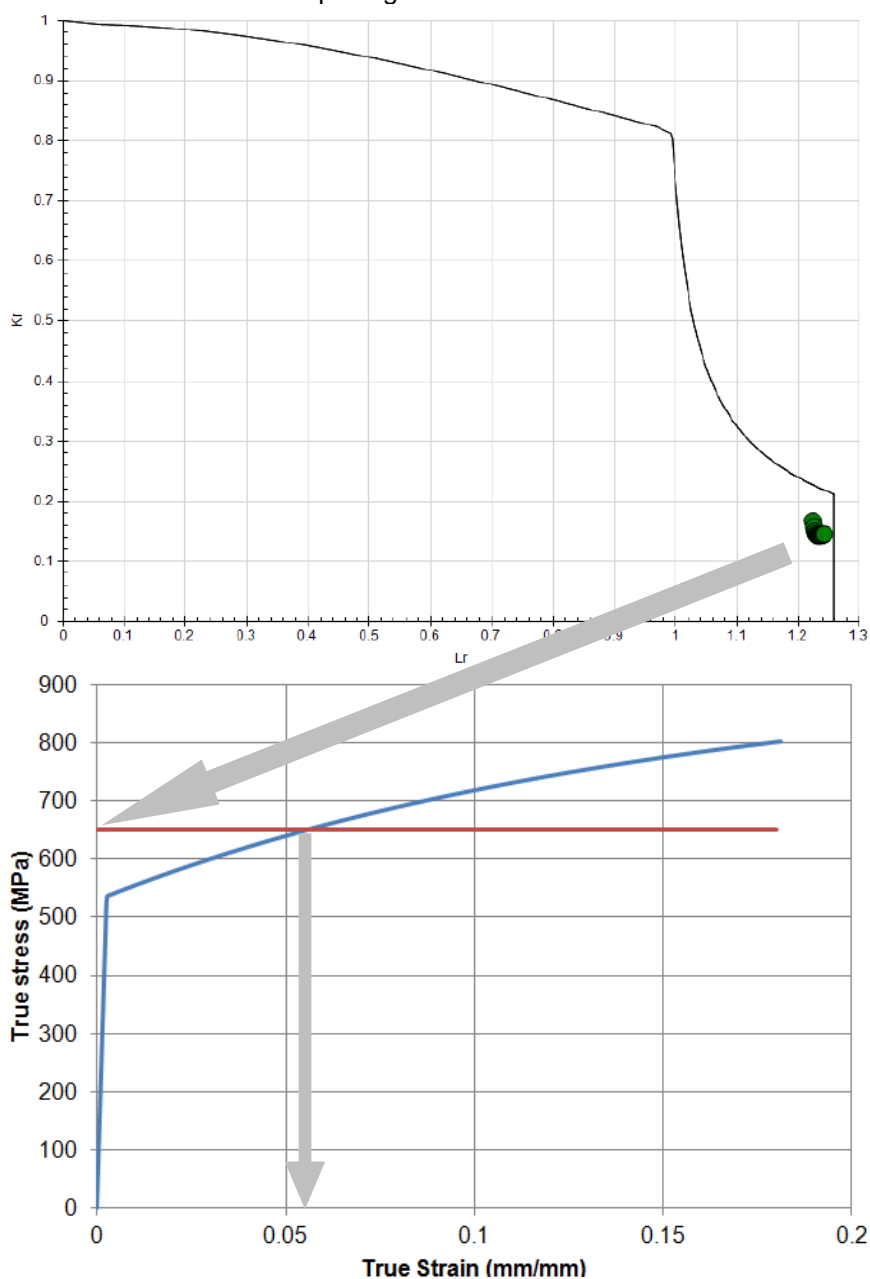


Figure 36 - BS7910:2005 Level 3B (ductile tearing) assessment.

## 7.6 Tangency Analysis Approach (ExxonMobil)

A series of ten numerical analyses has been performed based on the case of the flawed pipe described in Figure 28. The meshes are shown in Figure 37. The commercial software ABAQUS was used *via* with a Python routine to automate the mesh operation. Due to symmetries, only  $\frac{1}{4}$  of the pipe was actually meshed with about 80'000 3D linear elements (eight nodes) using full integration (c3d8). Large deformation theory was applied. The loading consists of two steps. In a first step, an internal pressure  $P = 0.80 \cdot P_c$  is applied, where  $P_c$  is given by:

$$P_c = \frac{2t}{R_{ID} + R_{OD}} \sigma_{flow} \quad (10)$$

where  $\sigma_{flow} = 450$  MPa,  $t = 22.2$  mm,  $R_{ID} = 139.70$  mm and  $R_{OD} = 161.90$  mm, *i.e.*  $P = 51.8$  MPa. In a second step, the internal pressure is maintained and a displacement is prescribed at the remote section in the axial direction of the pipe. The applied strain value was extracted as an average strain measured as the displacement of two nodes distant of  $L_0 = 300$  mm. An elastic beam was meshed to model the double clip gauges, and the CTOD was extracted as a combination of the displacement of two nodes located 2 mm and 8 mm above the crack mouth, using equation 10.

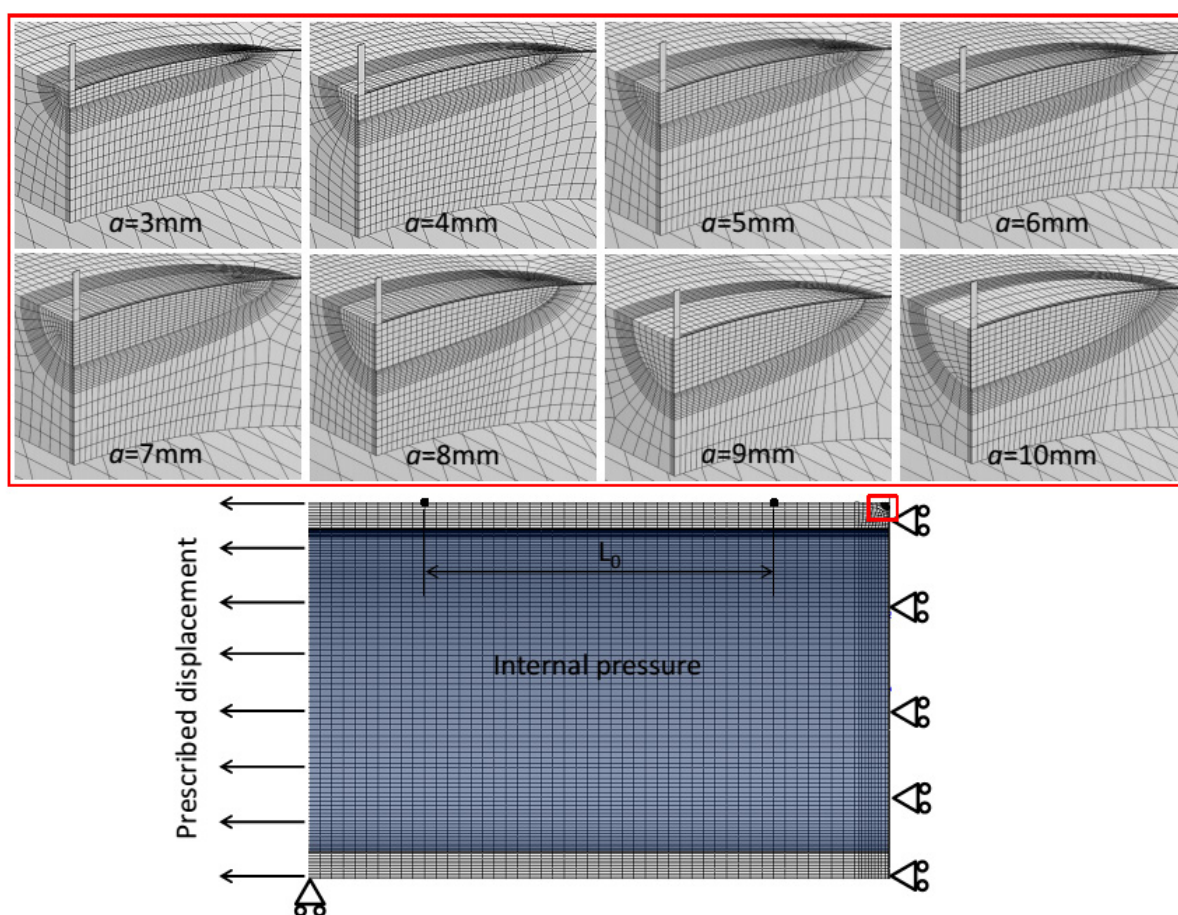


Figure 37 - Meshes for the crack driving force approach.

In order to check the consistency of the FEA results, comparisons have been made between the analytical solutions given by ExxonMobil Level 1 and 2 assessments. These models derived from a series of more than 90 full-scale tests. The results following ExxonMobil models are given in Table 5.

	Level 1		Level 2	
	1	1	2	3
<b>R-curve</b>				
<b>Pipe Y/T</b>	0.92	0.92	0.92	0.92
<b>Pipe UEL</b>	6 %	12 %	12 %	12 %
<b>Mismatch</b>	18.67 %	18.67 %	18.67 %	18.67 %
<b>Misalignment</b>	3 mm	0 mm	0 mm	0 mm
<b>Pressure</b>	80 %	80 %	80 %	80 %
<b>Critical strain <math>\epsilon_c</math></b>	<b>1.52 %</b>	<b>3.52 %</b>	<b>4.88 %</b>	<b>6.09 %</b>

Table 5 - Critical strain as calculated using ExxonMobil Level 1 and 2 assessments.

As evidenced on Figure 38, the critical strain determined by the tangency analysis is 5.5%. The results are consistent with level 2 analytical models proposed by ExxonMobil.

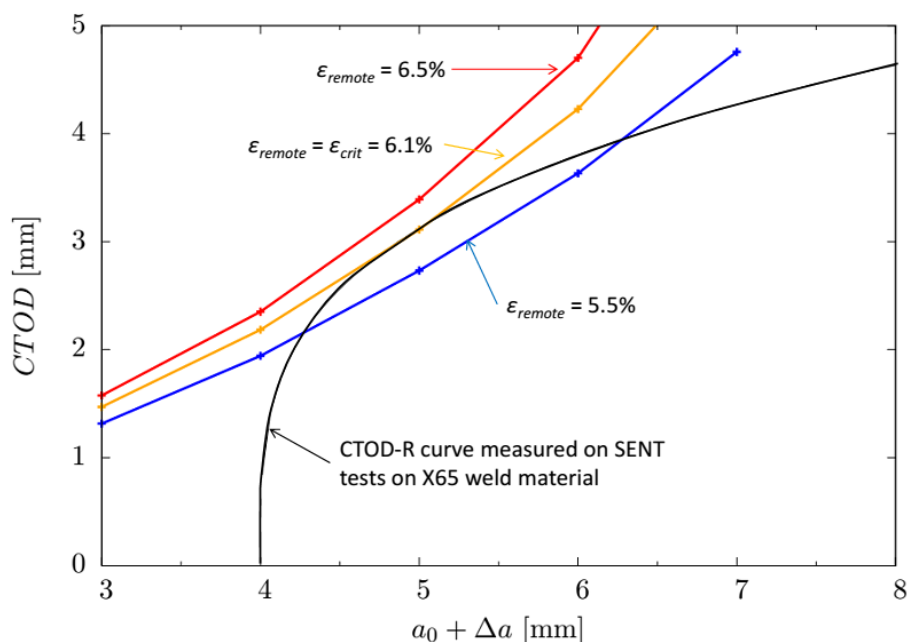


Figure 38 - Tangency analysis applied to the cracked pipe as described in Figure 28.

### 7.7 Local approach

#### 7.7.1 Formulation

In this paper, the GTN model has been used. The initial porosity  $f_0$  has been taken equal to 0.0004 for the base material and equal to 0.00005 for the weld material, which is consistent with the values found in the literature for these materials.  $q_1$  and  $q_2$  parameters have been identified on  $NT_x$  specimens using the inverse method.

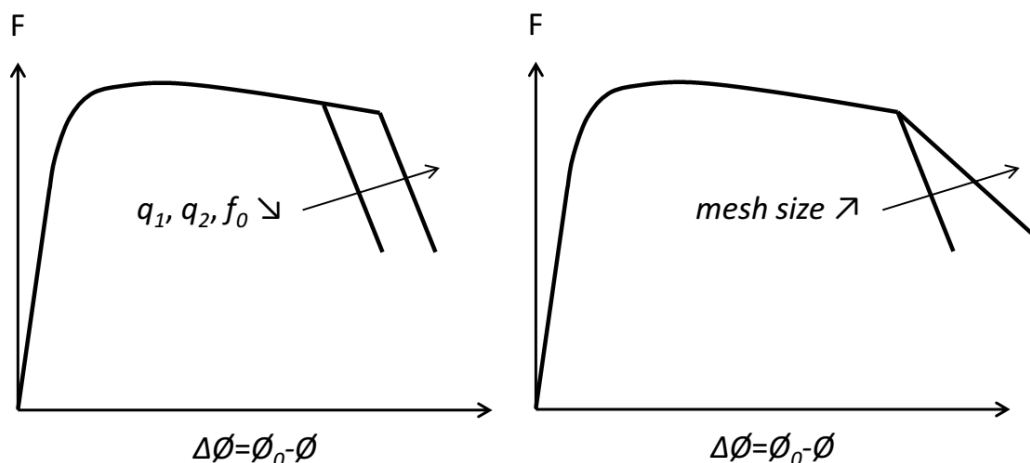


Figure 39 - Effect of the GTN model parameters  $q_1$ ,  $q_2$  and  $f_0$ ; and effect of the mesh size dependency.

The typical effect of the GTN model parameters on a displacement-load curve of a NT test is depicted in Figure 39. Also, one can see the effect of the mesh size on the crack propagation velocity. For the considered materials, a size of 200  $\mu\text{m}$  allowed good fit with experimental data.

The identified values of the GTN model parameters are given in Table 6 for both base material and weld material, and a comparison between experimental and simulated curves is given in Figure 40.

	$q_1$	$q_2$	$f_0$
<b>Base material (X65)</b>	1.589	1.023	0.0004
<b>Weld material</b>	1.716	1.206	0.00005

Table 6 - GTN model parameters for the X65 base material and weld material.

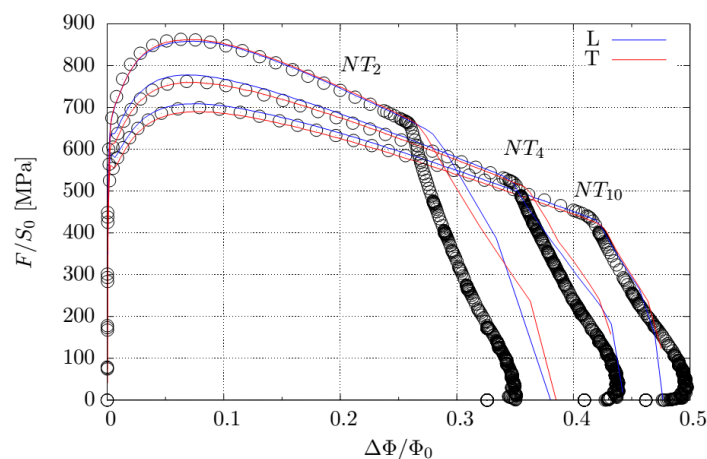
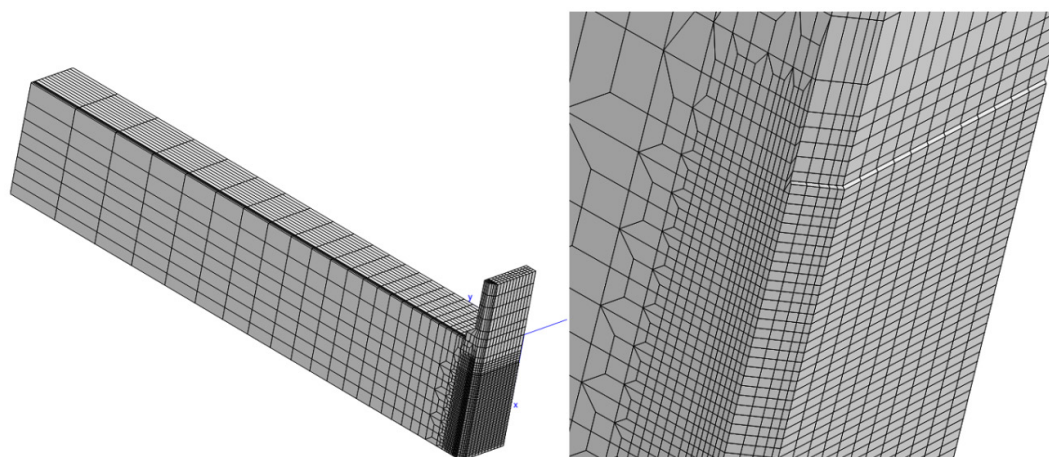


Figure 40 - The notched tensile tests simulated with the GTN model show a good fit with the experimental data.

### 7.7.2 Validation of the GTN model

Simulations have been carried out on SENT specimens in order to validate the GTN model. The finite element model is shown in Figure 41. Due to symmetries; only  $\frac{1}{4}$  of the specimen was actually meshed. All the calculations were performed using 3D linear elements (eight nodes) using full integration. The size of the elements within the crack growth region is equal to  $200\ \mu\text{m}$ , as identified on  $\text{NT}_x$  specimens. The transition from the fine meshed region at the vicinity of the crack tip to the coarse meshed region away from the crack tip is achieved using a structured transitional mesh pattern. Also, much thinner elements were defined near the free surface to accommodate the reduced constraint in that region. Since the element size at the crack tip is higher than the actual crack tip radius ( $55\ \mu\text{m}$ ), the crack tip shape is not  $\frac{1}{4}$  circle. This mesh gave good results in terms of elastic-plastic response. Finally, two elastic beams model the double clip gauge system.

Figure 41 -  $\frac{1}{4}$  FE mesh of a SENT with side-grooves

Two loading cases were considered. First, the specimen was loaded under displacement controlled loading up to the failure. It enabled to validate the GTN model. Figure 42 shows that the numerical results match the experimental data. Here, for the sake of readability, only one set of experimental data is depicted.

In a second time, the specimen was loaded under displacement controlled loading using the unloading compliance method and the results were then processed using the same method as for experimental data. Results are given in Figure 42. From these, three observations are made:

1. The GTN model parameters identified on  $NT_x$  specimens enable a good fit between numerical results and experimental data,
2. The unloading compliance method does not affect the material response as shown by the good match between the two simulated CTOD-load curves (Figure 42),
3. FE analysis using GTN model can successfully represents an actual CTOD-R curve test carried out on a laboratory specimen, as shown by the comparison between the simulated and experimental CTOD- $\Delta a$  curve (Figure 43). Also, the comparison between calculated and actual crack shape after failure shows a good match.

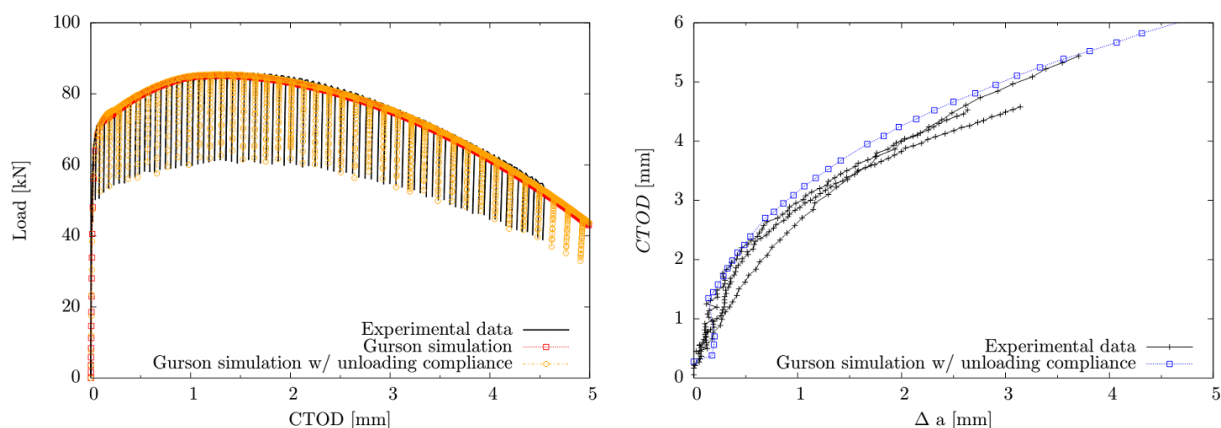


Figure 42 - Comparison between experimental data and numerical curves for the base material

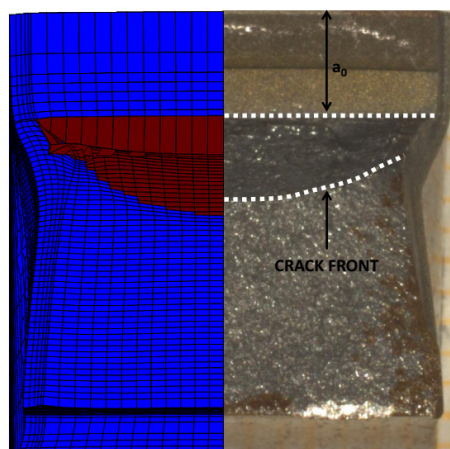


Figure 43 - Comparison between the final crack size  $a_f$  between experimental and GTN simulation. ( $CTOD = 3.4$  mm)

### 7.7.3 Engineering Critical Assessment on the pipe

The element size in the growth region was  $0.200 \times 0.200 \times 0.450$  mm, which is in agreement with the SENT simulation. Due to symmetries, only  $\frac{1}{4}$  of the pipe was actually meshed with about 80'000 3D linear elements (eight nodes) using full integration (c3d8) and large deformation theory was applied. The same loading sequence as in section 7.6 has been applied. The model is described in Figure 44.

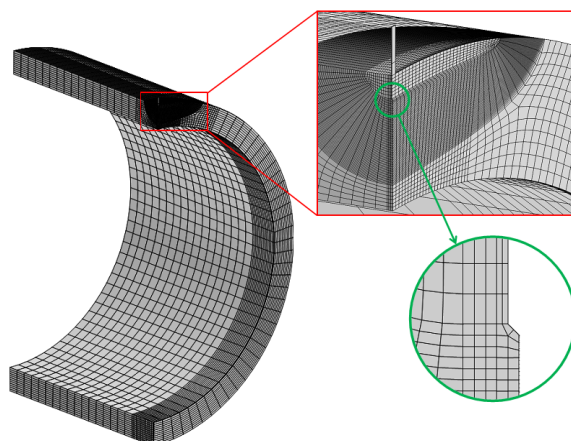


Figure 44 -  $\frac{1}{4}$  FE mesh of the pipe with an outer surface crack, and close up views of the mesh

## Results

Contrary to other approach (like FAD), the local approach does not imply an explicit failure criteria. Also, it is necessary to choose a criterion which to determine whether the structure is safe or not from failure. For example, a given amount of crack growth  $\Delta a_c$  at the centre of the crack may be chosen (see. Figure 45).

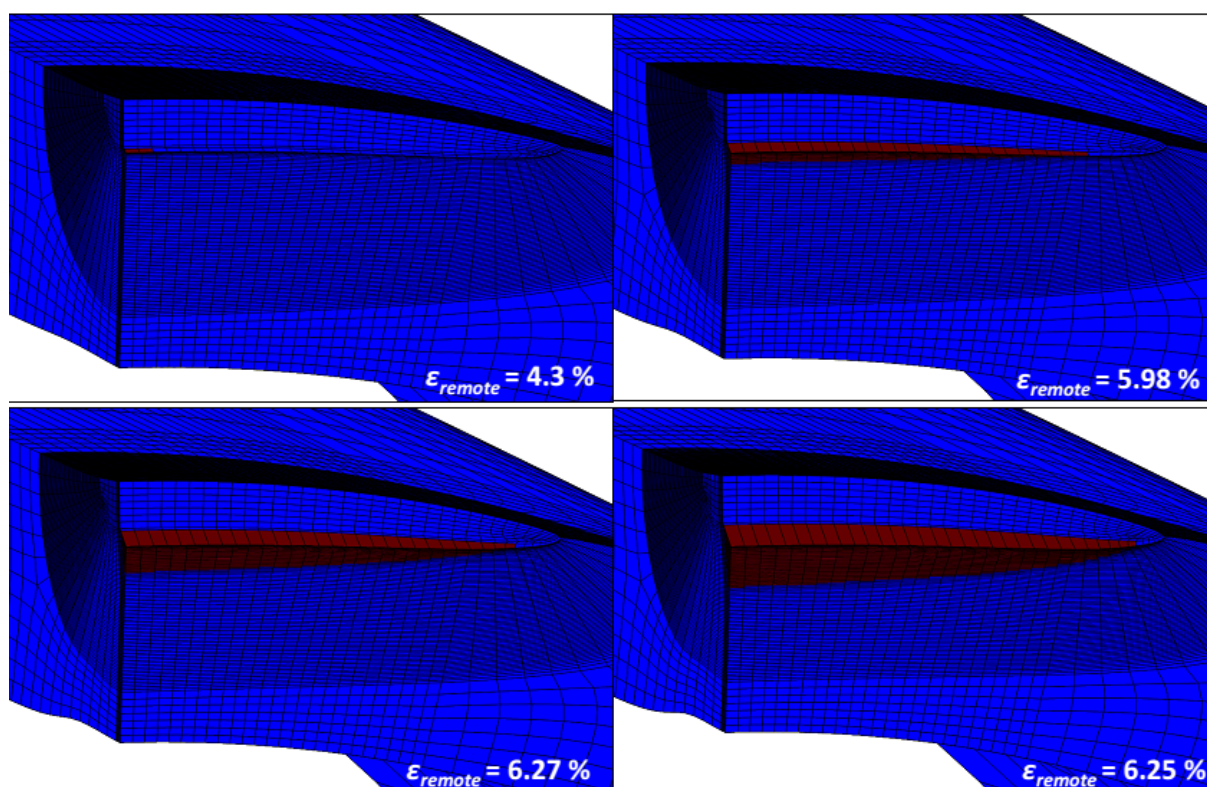


Figure 45 - Crack growth in the thickness direction as a function of the prescribed remote strain. The elements coloured in red correspond to the broken elements.

The crack propagation was plotted versus the applied strain in Figure 46.

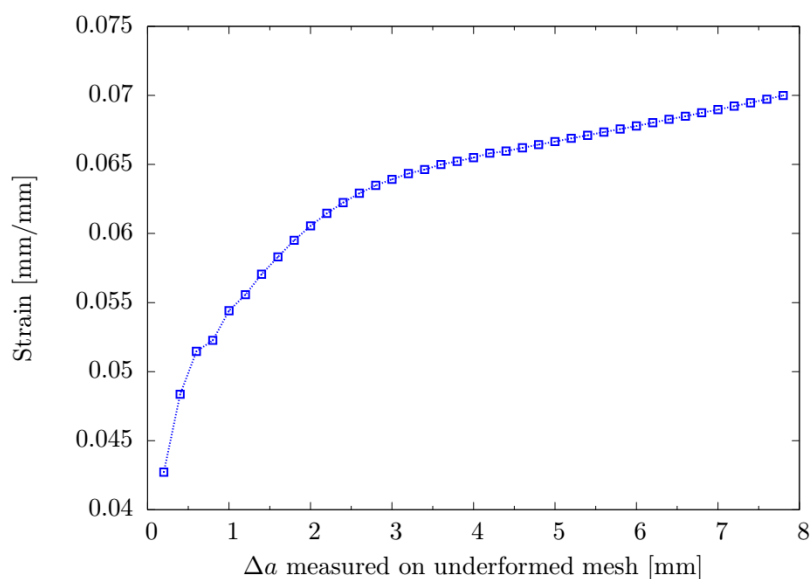


Figure 46 - Evolution of the strain as a function of the crack growth measured on the non deformed mesh.

## 7.8 Summary of ECA results

On the case selected for the purpose of this paper, the results are summarised in table 7.

	<b>FAD BS7910 – Level 3B</b>	<b>Tangency analysis</b>	<b>Local approach</b>
<b>Critical strain</b>	5.3%	5.5%	4.2% (crack initiation) 5.3% (1 mm propagation)
<b>Crack propagation</b>	1.5 mm	around 1 mm	see above
<b>Comments</b>	Results are very sensitive to material stress-strain curve. For embedded defect solution due to reference stress, the acceptable strain would be much lower.	From 1.5% to 6.1% depending on the level of selected ExxonMobil strain based design model	Allows capturing crack initiation and propagation.

Table 7 – Summary of ECA results

It can be evidenced that the results are quite homogeneous with the different approaches in terms of both critical strain and crack propagation. However, more comparisons would be required and especially comparisons for combined loading conditions, various  $a/W$  ratio ... for which more significant differences are expected.

As also highlighted by ExxonMobil in [26], FAD and tangency analysis approaches do not capture the physics of ductile tearing; where GTN model allows capturing this physics.

## 8. CONCLUSIONS

In this paper, the use of the SENT specimen in ECA for flawed pipelines is treated. It is shown that the SENT specimen conveniently replaces the CT and SENB specimens that exhibit over conservative R-curve due to the constraint effect. The J-Q approach developed in this paper confirms that the SENT presents a good transferability with regards to the pipe in terms of crack tip constraint. Also, one shall consider the use of this specimen when the material toughness must be defined.

Then, all questions and issues related to the various approaches for strain based design ECA (FAD, tangency analysis and local approach) are discussed.

Table 7 summarizes the main issues with the different methods.

	<b>Material testing</b>	<b>SENT test (fracture toughness determination)</b>	<b>Engineering Critical Assessment</b>
<b>FAD</b>	No issue (standard test)	$a/W$ ratio shall be properly chosen at least for level 3 assessments.	Method originally not developed for strain based design. How to account for biaxial loading conditions can be a subject of discussions. Strong sensitivity of the assessment line to material stress-strain curve. BS7910 embedded defects solution might be highly conservative in strain based design application.
<b>Tangency analysis</b>	No issue (standard test).	The determination of the $J$ - $R$ curve from one test is not standardised (6 tests required). Even if it is shown that the unloading compliance method is acceptable, it shall be standardised to be able to use the method on a regular basis.	Where CTOD is used instead of $J$ , consistency shall be ensured between SENT test analysis and pipe calculations. Where $J$ -integral is used several points shall be checked (validity of the $J$ -integral calculation). The crack driving force determination is not fully satisfactory.
<b>Local approach</b>	Non standard tests (notched tensile specimens)	No issue. SENT specimen is not used for model calibration but for model validation.	Mesh size is a model parameter. Acceptance criteria shall be defined for acceptable crack propagation.
<i>The effect of welding residual stresses has not been discussed but it is deemed not critical for strain based design due to welding residual stress relaxation by plastic deformation</i>			

Table 7 – Summary of main issues with the various possible ECA methods

Finally, the three ECA methods are compared on one example. This example shows that the three methods give quite similar results but this comparison is obviously only a very first step and additional comparisons including experimental results are of interest.

## 9. REFERENCES

- [1] *BS 7910: Guide to methods for assessing the acceptability of flaws in metallic structures*. British Standard Institution, 2005.
- [2] *RP-F108: Fracture control for pipeline installation methods introducing cyclic plastic strain*. Det Norske Veritas, 2006.
- [3] *ASTM A 370 : Standard Test Methods and Definitions for Mechanical Testing of Steel Products*, ASTM, 2012.
- [4] *OS-F101: Offshore Standard*. Det Norske Veritas, 2013.
- [5] *ASTM E 1820-06: Standard Test Method for Measurement of Fracture Toughness*. ASTM, 2006.
- [6] *BS 7448: Fracture mechanics toughness tests*. British Standard Institution, 1991.
- [7] Chiesa, M, Nyhus B, Skallerud B, Thaulow C (2001): *Efficient fracture assessment of pipelines. A constraint-corrected SENT specimen approach*. Engineering Fracture Mechanics, **68**, pp.527-547.
- [8] Hutchinson, JW (1968): *Singular behaviour at the end a tensile crack in a hardening material*. Journal of the Mechanics and Physics of Solids, **16**, pp.13-31.
- [9] Rice, JR, Rosengren, GF (1968): *Plane strain deformation near a crack tip in a power-law hardening material*. Journal of the Mechanics and Physics of Solids, **16**, pp.1-12.

- [10] Sharma, SM, Aravas, N (1991): *Determination of higher order terms in asymptotic elastoplastic crack tip solutions*. Journal of Mechanics and Physics of Solids, **39**, pp.1043-1072.
- [11] O'Dowd, NP, Shih, CF (1991): *Family of crack-tip fields characterized by a triaxiality parameter-I*. Journal of Mechanics and Physics of Solids, **39**, pp.989-1015.
- [12] Zhu, X-K, McLaughy T, Orth, F, Jennings, J (2014): *Review of Low-Constraint Fracture Resistance Testing with SENT Specimens*. Proceedings of the ASME 2014 33<sup>rd</sup> International Conference on Ocean, Offshore and Arctic Engineering OMAE 2014. Paper 24281.
- [13] Nyhus, B, Østby, E, Knagenhjelm, HO, Black, S, Rostadsand, PA (2005): *Experimental studies on the effect of crack depth and asymmetric geometries on the ductile tearing resistance*. Proceedings of the ASME 2005 24<sup>th</sup> International Conference on Ocean, Offshore and Arctic Engineering OMAE 2005. Paper 67532.
- [14] Kang, J, Shen, G, Liang, J, Gianetto, J (2014): *Influence of Constraint on J-Resistance Curve for an X100 Pipe Steel*. 20<sup>th</sup> European Conference on Fracture (ECF20). Procedia Materials Science, **3**, pp.239-244.
- [15] Moore, P (2014): *The effect of notch sharpness on the fracture toughness determined from SENT specimens*. Proceedings of the ASME 2014 33<sup>rd</sup> International Conference on Ocean, Offshore and Arctic Engineering OMAE 2014. Paper 24663.
- [16] Cravero, S, Ruggieri, C (2007): *Estimation procedure of J-resistance curves for SE(T) fracture specimens using unloading compliance*. Engineering Fracture Mechanics, **74**, pp.2735-2757.
- [17] *RCC-MR Annexe A16: Guide pour les études de fuite avant rupture et les analyses de nocivité de défauts associées*. AFCEN, 2007.
- [18] Newman, JC, Raju, IS (1981): *An Empirical Stress-Intensity Factor Equation for the Surface Crack*. Engineering Fracture Mechanics, **15**, 1-2, pp.182-195.
- [19] Rice, J.E. (1968): *A path independent integral and the approximate analysis of strain concentrations by notches and cracks*. Journal of Applied Mechanics, **35**, pp.379-386.
- [20] Østby, E, Thaulow, C, Nyhus, B (2007): *A new approach to ductile tearing assessment of pipelines under large-scale yielding*. International Journal of Pressure Vessels and Piping, **84**, pp.337-348.
- [21] ExxonMobil Upstream Research Company: *Measurement of Crack-Tip Opening Displacement (CTOD) Fracture Resistance Curves Using Single-Edge Notched Tension (SENT) Specimens*, 2010.
- [22] Wells, A.A. (1961): *Unstable crack propagation in metals: cleavage and fast fracture*. Proceedings of the crack propagation symposium, **1**, paper number 84.
- [23] Ernst, HA, Paris, PC and Landes, JD (1981): *Estimation on J-integral and Tearing Modulus T from a Single Specimen Test Record*. Fracture Mechanics, 13<sup>th</sup> Conference, ASTM STP 743, ASTM International, West Conshohocken, PA, pp.476-502.
- [24] Shih, CF (1981): *Relationship between the J-integral and crack opening displacement for stationary and growing cracks*. Journal of Mechanics and Physics of Solids, **29**, pp.305-326.
- [25] Moore, P.L. and Pisarski, H.G., 2012, *Validation of Methods to Determine CTOD from SENT Specimens*. Proceedings of the 22nd International Ocean and Polar Engineering Conference, Rhodes, Greece.
- [26] Tang, H, Fairchild D., Panico M., Crapps J., Cheng W.: *Strain capacity prediction of strain based design pipeline*. IPC 2014-33749.